

1 **TITLE: A human antibody reveals a conserved site on beta-coronavirus spike**  
2 **proteins and confers protection against SARS-CoV-2 infection**  
3

4 **SUMMARY: A human mAb isolated from a COVID-19 donor defines a protective**  
5 **cross-neutralizing epitope for pan- $\beta$ -CoV vaccine design strategies**  
6

7 **AUTHORS:**

8 Panpan Zhou<sup>1,3,4,\*</sup>, Meng Yuan<sup>2,\*</sup>, Ge Song<sup>1,3,4,\*</sup>, Nathan Beutler<sup>1,\*</sup>, Namir Shaabani<sup>1,\*</sup>,  
9 Deli Huang<sup>1</sup>, Wan-ting He<sup>1,3,4</sup>, Xueyong Zhu<sup>2</sup>, Sean Callaghan<sup>1,3,4</sup>, Peter Yong<sup>1,3,4</sup>, Fabio  
10 Anzanello<sup>1,3,4</sup>, Linghang Peng<sup>1</sup>, James Ricketts<sup>1</sup>, Mara Parren<sup>1</sup>, Elijah Garcia<sup>1</sup>, Stephen  
11 A. Rawlings<sup>5</sup>, Davey M. Smith<sup>5</sup>, David Nemazee<sup>1</sup>, John R. Teijaro<sup>1</sup>, Thomas F.  
12 Rogers<sup>1,5,†</sup>, Ian A. Wilson<sup>2,3,4,6,†</sup>, Dennis R. Burton<sup>1,3,4,7,†</sup>, Raiees Andrabi<sup>1,3,4,†</sup>  
13

14 **AUTHOR AFFILIATIONS:**

15 <sup>1</sup>Department of Immunology and Microbiology, The Scripps Research Institute, La Jolla,  
16 CA 92037, USA.

17 <sup>2</sup>Department of Integrative Structural and Computational Biology, The Scripps Research  
18 Institute, La Jolla, CA 92037, USA.

19 <sup>3</sup>IAVI Neutralizing Antibody Center, The Scripps Research Institute, La Jolla, CA 92037,  
20 USA

21 <sup>4</sup>Consortium for HIV/AIDS Vaccine Development (CHAVID), The Scripps Research  
22 Institute, La Jolla, CA 92037, USA.

23 <sup>5</sup>Division of Infectious Diseases, Department of Medicine, University of California, San  
24 Diego, La Jolla, CA 92037, USA.

25 <sup>6</sup>Skaggs Institute for Chemical Biology, The Scripps Research Institute, La Jolla, CA  
26 92037, USA.

27 <sup>7</sup>Ragon Institute of Massachusetts General Hospital, Massachusetts Institute of  
28 Technology, and Harvard University, Cambridge, MA 02139, USA.

29 \*These authors contributed equally to this work.

30 †Corresponding author. Email: trogers@scripps.edu (T.F.R.); wilson@scripps.edu  
31 (I.A.W); burton@scripps.edu (D.R.B.); andrabi@scripps.edu (R.A.).  
32  
33  
34

35 **ABSTRACT**

36

37 Broadly neutralizing antibodies (bnAbs) to coronaviruses (CoVs) are valuable in their own  
38 right as prophylactic and therapeutic reagents to treat diverse CoVs and, importantly, as  
39 templates for rational pan-CoV vaccine design. We recently described a bnAb, CC40.8,  
40 from a coronavirus disease 2019 (COVID-19)-convalescent donor that exhibits broad  
41 reactivity with human beta-coronaviruses ( $\beta$ -CoVs). Here, we showed that CC40.8 targets  
42 the conserved S2 stem-helix region of the coronavirus spike fusion machinery. We  
43 determined a crystal structure of CC40.8 Fab with a SARS-CoV-2 S2 stem-peptide at 1.6  
44 Å resolution and found that the peptide adopted a mainly helical structure. Conserved  
45 residues in  $\beta$ -CoVs interacted with CC40.8 antibody, thereby providing a molecular basis  
46 for its broad reactivity. CC40.8 exhibited in vivo protective efficacy against SARS-CoV-2  
47 challenge in two animal models. In both models, CC40.8-treated animals exhibited less  
48 weight loss and reduced lung viral titers compared to controls. Furthermore, we noted  
49 CC40.8-like bnAbs are relatively rare in human COVID-19 infection and therefore their  
50 elicitation may require rational structure-based vaccine design strategies. Overall, our  
51 study describes a target on  $\beta$ -CoV spike proteins for protective antibodies that may  
52 facilitate the development of pan- $\beta$ -CoV vaccines.

53

54 **MAIN TEXT**

55 **Introduction**

56

57 Severe acute respiratory syndrome coronavirus 2 (SARS-CoV-2) has led to the current  
58 global pandemic (1-3). SARS-CoV-2 is a virus that belongs to the coronaviridae family of  
59 which six members have previously crossed into humans from animal reservoirs and  
60 established widespread infections (4, 5). These include four endemic human  
61 coronaviruses (HCoVs) (HCoV-229E, HCoV-HKU1, HCoV-OC43, HCoV-NL63)  
62 responsible for non-severe, seasonal infections (4) as well as SARS-CoV-1 and MERS-  
63 CoV (Middle East Respiratory Syndrome CoV) that are associated with high morbidity  
64 and mortality in humans (6, 7). Among the seven HCoVs, SARS-CoV-2 closely resembles  
65 SARS-CoV-1 and, to lesser degree, MERS-CoV. Together with HCoV-HKU1 and HCoV-  
66 OC43, these viruses belong to the *β-coronavirus* genus (4, 5). SARS-CoV-2 is highly  
67 transmissible in humans and causes coronavirus disease-2019 (COVID-19), associated  
68 with severe respiratory failure leading to high morbidity and a reported mortality of about  
69 0.7 to 2% of infected individuals worldwide (2, 8, 9). There are considerable concerns that  
70 future coronavirus spillovers will trigger new pandemics (10-15).

71

72 Coronavirus pandemic preparedness may consider responses through establishment of  
73 techniques for rapid generation of specific reagents to counter the emerging coronavirus  
74 and control spread. An alternative is to seek to identify broadly neutralizing antibodies  
75 (bnAbs) to coronaviruses and use molecular information gleaned on their epitopes to  
76 rationally design pan-coronavirus vaccines (16-18). Pan-coronavirus vaccines and

77 antibodies could be stockpiled ahead of the emergence of a new coronavirus and used  
78 to rapidly contain the virus. BnAbs and pan-coronavirus vaccines that target more  
79 conserved regions of the virus may also be more effective against antigenically variant  
80 viruses, such as have been described for the variants of concern in the COVID-19  
81 pandemic (19-22).

82

83 All HCoV possess a surface envelope spike glycoprotein that mediates interaction with  
84 host cell receptors and enables virus fusion (4, 23). SARS-CoV-2 (similar to SARS-CoV-  
85 1) utilizes the receptor binding domain (RBD) in the S1 subunit of the spike protein to  
86 engage human angiotensin converting enzyme 2 (hACE2) on host cells for cell entry and  
87 infection (23-27). The SARS-CoV-2 spike glycoprotein is the primary target of neutralizing  
88 antibodies (nAbs) (28-31). On the spike protein, the RBD is highly immunogenic and is  
89 recognized by the majority of nAbs (28, 32-43), and thus is a major focus of current nAb-  
90 based vaccine design efforts (28, 44, 45). However, due to sequence diversity, cross-  
91 reactivity to the RBD region is limited, especially among emerging coronaviruses with  
92 pandemic potential (10-13). The most potent nAbs in humans during natural infection are  
93 typically raised to epitopes overlapping the ACE2 binding site (32, 33, 42, 45, 46). As the  
94 rapid spread of the SARS-CoV-2 virus continues, these epitopes are coming under strong  
95 immune selection pressure at the population level, leading to the selection of SARS-CoV-  
96 2 neutralization escape variants (19-22, 47-49). The relevant mutations may result in  
97 reduced effectiveness of vaccine-induced antibody responses in humans since such  
98 responses also tend to target RBD epitopes overlapping the ACE2 binding site, and  
99 because all currently approved vaccines are based on the wild-type virus. The most

100 striking example that illustrates the capability of the RBD to mutate without majorly  
101 affecting the ability of the virus to engage host receptor is the variability of the RBD across  
102 the two families of HCoVs: SARS-CoV-2/1 ( $\beta$ -HCoVs) and HCoV-NL63 ( $\alpha$ -HCoV) (23-27,  
103 50). These HCoVs possess divergent RBDs, but all use the ACE2 receptor for viral entry  
104 suggesting that SARS-CoV-2, and potentially other emerging sarbecoviruses with human  
105 pandemic potential, can tolerate changes in this domain with limited fitness cost.  
106 Therefore, we believe that other sites on the spike protein should be explored as targets  
107 of bnAbs.

108

109 We recently isolated a SARS-CoV-1/2 cross-neutralizing antibody from a COVID-19  
110 donor, CC40.8, that exhibits broad cross-reactivity with human  $\beta$ -CoVs (51). Here, we  
111 show that the CC40.8 bnAb targets an S2 stem-helix epitope, which is part of the  
112 coronavirus fusion machinery. We first identified a long 25-mer S2 peptide from HCoV-  
113 HKU1 that bound CC40.8 with high affinity and then determined the crystal structure of  
114 CC40.8 with the SARS-CoV-2 S2 peptide. The S2 stem peptide adopts a largely helical  
115 structure that is embedded in a groove between the heavy and light chain  
116 complementarity determining regions (CDRs) of the antibody. Key epitope contact  
117 residues were further validated, by alanine scanning, to be important for peptide binding  
118 and for virus neutralization. These contact residues are largely conserved between  $\beta$ -  
119 CoVs, consistent with the cross reactivity of CC40.8. In SARS-CoV-2 challenge models,  
120 CC40.8 showed in vivo protective efficacy by reducing weight loss and lung tissue viral  
121 titers. Although two recent studies have described S2-stem nAbs isolated from mice and  
122 mice transgenic for human Ig (52, 53), CC40.8 represents a human HCoV S2-stem

123 directed bnAb isolated from natural infection (51) and may facilitate development of  
124 antibody-based interventions and prophylactic pan-sarbecovirus and pan- $\beta$ -coronavirus  
125 vaccine strategies.

126

127 **Results**

128

129 **CC40.8 binds a conserved peptide from the S2 region of  $\beta$ -coronaviruses.**

130

131 We recently isolated a bnAb, CC40.8, from a 62-year-old SARS-CoV-2 convalescent  
132 donor from peripheral blood mononuclear cell (PBMC) samples collected 32 days post-  
133 infection (51). CC40.8 bnAb neutralizes SARS-CoV-1 and SARS-CoV-2 and exhibits  
134 broad reactivity against  $\beta$ -coronaviruses, notably the endemic coronavirus HCoV-HKU1  
135 (Fig. 1A and B) (51). Here, we observed that CC40.8 bnAb can effectively neutralize clade  
136 1b and clade 1a ACE2 receptor-utilizing sarbecoviruses (Fig. 1A, fig. S1A). In addition,  
137 the CC40.8 bnAb was consistently effective against the current SARS-CoV-2 variants of  
138 concern (VOCs) (Fig. 1A, fig. S1A). The effectiveness of CC40.8 bnAb with SARS-CoV-  
139 2 VOCs is consistent with a lack of mutations in the S2 stem helix region in the current  
140 VOCs (21). To assess the cell-cell inhibition ability of CC40.8 bnAb, we conducted  
141 experiments in HeLa cells expressing SARS-CoV-2 spike protein or hACE2 receptor. We  
142 observed that CC40.8 bnAb can prevent cell-cell fusion of HeLa cells expressing SARS-  
143 CoV-2 spike protein with HeLa cells expressing the hACE2 receptor (fig. S2).

144

145 Using negative-stain electron microscopy (ns-EM), we previously showed that the CC40.8  
146 antibody targets the base of the S2 subunit on HCoV spike proteins, but epitope flexibility  
147 precluded determination of a high-resolution structure (51). Here, we pursued epitope  
148 identification, first by peptide mapping. Using HCoV-HKU1 S2 subunit overlapping  
149 biotinylated peptides (15-residue long with a 10-residue overlap) for binding to CC40.8,

150 we identified that the stem-helix region in the S2 fusion domain contains the epitope (Fig.  
151 1C, fig. S3). Then, through screening with peptides of various lengths that include the  
152 epitope, we identified a 25-residue peptide that showed the strongest binding by biolayer  
153 interferometry (BLI, Fig. 1D). The peptide corresponds to residues 1226-1250 from the  
154 HCoV-HKU1 S2 sequence.

155  
156 Next, we tested BLI binding of CC40.8 bnAb with peptides encompassing similar S2-  
157 domain regions of other HCoVs. We observed that the antibody binds to the  $\beta$ - but not to  
158 the  $\alpha$ -HCoV S2-domain peptides (Fig. 1D). This pattern is consistent with the differential  
159 binding of CC40.8 bnAb to different families of HCoV spike proteins (Fig. 1B) (51).  
160 Sequence alignment of the S2 stem-helix domain region showed strong conservation  
161 between SARS-CoV-1 and SARS-CoV-2 with more modest conservation across the  
162 seasonal  $\beta$ -CoVs, consistent with cross-reactive binding patterns (Fig. 1E to G).

163  
164 To determine whether CC40.8 bnAb affinity maturation was important for cross-reactive  
165 binding or neutralization, we generated an inferred germline (iGL) version of CC40.8 with  
166 corresponding antibody V-D-J germline genes (fig. S1B), as described previously (54,  
167 55). Although the CC40.8 bnAb iGL Ab version retained binding to spike proteins and the  
168 stem-helix peptides of  $\beta$ -CoVs, the neutralizing activity was lost against sarbecoviruses  
169 (fig. S1, C to E), suggesting that affinity maturation is critical for neutralization, but cross-  
170 reactive breadth is germline-encoded. Interestingly, the CC40.8 iGL bnAb showed binding  
171 to MERS-CoV spike protein that CC40.8 bnAb fails to bind and exhibited some weak

172 polyreactivity (fig. S1, fig. S4), suggesting that naive B cells targeting this epitope may  
173 begin with a broader reactivity to CoV spike proteins.

174

175 **The epitope of CC40.8 bnAb was defined by the crystal structure of a peptide-**  
176 **antibody complex.**

177

178 To investigate the molecular nature of the CC40.8 bnAb epitope, we determined the 1.6  
179 Å resolution crystal structure of the antibody Fab fragment with the SARS-CoV-2 25-mer  
180 S2 peptide (Fig. 2A, table S1). The peptide adopts a largely helical structure that traverses  
181 a wide hydrophobic groove formed between the heavy and light chains of the Fab (fig.  
182 S5). The buried surface area on the peptide is about 1150 Å<sup>2</sup> (669 Å<sup>2</sup> conferred by the  
183 heavy chain and 488 Å<sup>2</sup> by the light chain) and is largely contributed by hydrophobic  
184 residue interactions at the paratope-epitope interface, although some hydrogen bonds  
185 and salt bridges are contributed by CDRHs1 to 3, FRH1, and CDRLs1 to 3 (Fig. 2A to C,  
186 fig. S6). Two peptide stretches of <sup>1142</sup>QPELD<sup>1146</sup> and <sup>1151</sup>ELDKYF<sup>1156</sup> and several nearby  
187 residues, F<sup>1148</sup> N<sup>1158</sup>, H<sup>1159</sup>, form the epitope of the bnAb (Fig. 2B and C). Notably,  
188 hydrophobic residues in <sup>1151</sup>ELDKYF<sup>1156</sup> of the stem region, as well as two upstream  
189 residues, L<sup>1145</sup> and F<sup>1148</sup>, form the core of the epitope that interacts with a hydrophobic  
190 groove in the antibody lined by heavy chain residues (V33, Y35, W47, Y56, Y58, M96  
191 and V101) and light chain residues (Y32, Y34, L46 and Y49) (Fig. 2C and fig. S6).  
192 Antibody germline and mutated residues both contribute to epitope recognition (fig. S6).  
193 Consistent with our findings, two recent independent studies have shown that  
194 heterologous CoV spike protein immunizations in mice or mice transgenic for the human

195 Ig locus can induce cross-reactive serum neutralizing antibodies that target the conserved  
196 S2 spike epitope similar to the stem-helix epitope identified in our study, and some  
197 isolated mAbs also show broad reactivity to coronavirus spike proteins (52, 53).

198

199 The residues important for CC40.8 interaction with virus were also investigated by alanine  
200 scanning mutagenesis of SARS-CoV-2 and HCoV-HKU1 peptides and spike protein by  
201 antibody binding and by neutralization of SARS-CoV-2 spike protein mutants (Fig. 2D and  
202 E, fig. S7). The contact residues determined by crystallography were also found to be  
203 important for peptide binding and neutralization with the S2 helical residues, L<sup>1145</sup>, E<sup>1151</sup>,  
204 F<sup>1148</sup> and Y<sup>1155</sup>, being the most critical (fig. S7). We noted some differences in CC40.8  
205 dependence on S2 residue substitutions for virus neutralization and spike protein binding,  
206 which may reflect differences in conformation or glycosylation between recombinant and  
207 native membrane-associated spike protein (56, 57). The conservation of those residues  
208 identified by crystallography and alanine scanning as most critical for interaction of  
209 CC40.8 with virus is high (Fig. 2F) across human  $\beta$ -coronaviruses and related  
210 sarbecoviruses that infect various animal species, thus providing a structural basis for  
211 broad cross-reactivity of the antibody.

212

213 The CC40.8 epitope region houses an N-linked glycan (N<sup>1158</sup>) that is highly conserved  
214 across coronaviruses and may restrict access to this bnAb epitope. To investigate, we  
215 substituted the T<sup>1160</sup> residue on SARS-CoV-2 virus spike protein with an alanine residue  
216 to eliminate the AsnHisThr (NHT) N-linked glycan attachment site. A modest increase in  
217 neutralization sensitivity of the T1160A variant relative to wild-type virus was observed

218 (Fig. 2E, fig. S7), suggesting that any steric obstruction of the epitope by the N1 158 glycan  
219 is limited.

220

221 The CC40.8 bnAb epitope appears to be only partially exposed on the pre-fusion HCoV  
222 spike protein (fig. S8). Previously, a SARS-CoV-2 S2 stem-targeting neutralizing  
223 antibody, B6, was isolated from a mouse immunized with spike protein (52) . Here we  
224 compared the structures of antibodies CC40.8 and B6 (fig. S9, A to E). Both antibodies  
225 target a similar epitope on the SARS-CoV-2 spike protein, the conserved S2 stem helix  
226 region, but with different angles of approach; a longer peptide was visualized as the  
227 epitope for CC40.8. The post-fusion spike protein requires a large conformational change  
228 in the S2 stem region, and the superimposed CC40.8 (fig. S8C) and B6 (52) would clash  
229 with the post-fusion conformation. On the other hand, if bound to a spike protein in the  
230 pre-fusion state, both antibodies would clash with the adjacent protomer (fig. S9, D and  
231 E), suggesting a possible neutralization mechanism where the antibodies may induce  
232 disruption of the S2 stem 3-helix bundle, and bind to an intermediate state of the spike  
233 protein (fig. S8C). This hypothesis is further supported by comparing the binding of  
234 CC40.8 to S2P and HexaPro (S6P). The two proline mutations (S2P) were introduced to  
235 stabilize the SARS-CoV-2 S trimer in its pre-fusion state (26, 58), whereas additional  
236 proline substitutions to the HexaPro or S6P construct further stabilized the SARS-CoV-2  
237 spike trimer (59). Here we show that the S6P-stabilized version exhibited much weaker  
238 binding to CC40.8 compared to S2P (fig. S9F), further suggesting that destabilization or  
239 partial disruption of the pre-fusion S trimer is a possible explanation for neutralization by  
240 S2 stem-targeting antibodies, such as CC40.8 or B6. Our previous EM study of the

241 complex of HCoV-HKU1 S (S2P) and CC40.8 Fab [Fig. 5D in ref (51)] showed high  
242 flexibility of the epitope and multiple antibody approach angles, which also suggested  
243 disruption of the 3-helix bundle and induction of flexibility in the S2 stem region.

244

245

246 **CC40.8 antibody protects against weight loss and reduces viral burden in SARS-**  
247 **CoV-2 challenge in vivo.**

248

249 To determine the in vivo efficacy of CC40.8, we conducted passive antibody transfer  
250 followed by SARS-CoV-2 challenge in human ACE2 (hACE2) mice and in Syrian  
251 hamsters. CC40.8 mAb at 4 different doses (300 $\mu$ g, 100 $\mu$ g, 50 $\mu$ g and 10 $\mu$ g per animal)  
252 was intra-peritoneally (i.p.) administered into groups (6 animals per group) of hACE2 mice  
253 (Fig. 3A) (60). An RBD nAb (CC12.1; 300  $\mu$ g/animal) positive control and a Zika-specific  
254 antibody (SMZAb1; 300  $\mu$ g/animal) negative control were administered i.p. into control  
255 animal groups. All CC40.8- and control mAb-treated animals were challenged with SARS-  
256 CoV-2 (USA-WA1/2020) by intranasal (i.n.) administration of a virus dose of  $2 \times 10^4$   
257 plaque forming units (PFU), 12 hours post-antibody infusion (Fig. 3A). The animals were  
258 weighed daily to monitor weight changes, as an indicator of disease due to infection and  
259 serum samples were collected to determine the transferred human antibody  
260 concentrations (Fig. S10). Animals were euthanized at day 5 and lung tissues were  
261 collected to determine the SARS-CoV-2 titers by quantitative polymerase chain reaction  
262 (qPCR) and by plaque assays. The CC40.8 bnAb-treated animals showed significantly  
263 reduced weight loss as compared to the SMZAb1-treated control group animals  
264 ( $P < 0.0001$ , Fig. 3B, fig. S10), suggesting a protective role for CC40.8. Remarkably, the

265 animals treated with the lowest dose of CC40.8 bnAb (10  $\mu$ g/animal) also showed  
266 significant protection against weight loss ( $P = 0.0005$ , Fig. 3B, fig. S10). As expected, the  
267 positive control RBD nAb, CC12.1 significantly protected against weight loss ( $P < 0.0001$ ,  
268 Fig. 3B, fig. S10). Consistent with these results, SARS-CoV-2 specific viral RNA copies  
269 and viral titers in day 5 lung tissues were significantly reduced in the CC40.8-treated  
270 animals compared to the SMZAb1 control group animals ( $P < 0.0001$ , fig. 3C and D).

271  
272 We also investigated the protective efficacy of CC40.8 mAb by intra-peritoneally (i.p.)  
273 administering into a group of 5 Syrian hamsters (at 2 mg per animal) and subsequently  
274 challenging with SARS-CoV-2 (USA-WA1/2020 dose of  $1 \times 10^6$  PFU) (fig. S11). SMZAb1  
275 Zika mAb was used as a control. Consistent with hACE2 mouse experiments, the CC40.8  
276 bnAb-treated animals showed substantially reduced weight loss and reduced SARS-CoV-  
277 2 titers in day 5 lung tissues demonstrating its protective role (fig. S11). Altogether, the  
278 findings reveal that CC40.8, despite relatively low in vitro neutralization potency, shows  
279 a substantial degree of protective efficacy against SARS-CoV-2 infection in vivo.  
280 Consistent with these results, a recently isolated S2 stem bnAb, S2P6, has also been  
281 shown to protect against SARS-CoV-2 challenge despite relatively low neutralization  
282 potency (61). Furthermore, this phenomenon of a surprisingly high degree of protection  
283 afforded by antibodies directed to epitopes close to the spike protein membrane and part  
284 of the fusion machinery has been described earlier for HIV (62).

285  
286 **The conserved stem-helix epitope defined by bnAb CC40.8 is infrequently targeted**  
287 **following SARS-CoV-2 infection.**

288

289 To investigate how frequently the CC40.8 epitope is targeted following SARS-CoV-2  
290 infection, we tested the binding of serum samples from 60 COVID-19 convalescent  
291 donors to 25-mer peptides of HCoV-229E corresponding to the stem-helix bnAb epitope. We  
292 observed that 6 of 60 (10%) individuals exhibited some degree of cross-reactive binding  
293 with  $\beta$ -HCoV S2 stem peptides (Fig. 4A). We further tested the binding of cross-reactive  
294 serum samples with SARS-CoV-2 S2 stem peptide alanine scan variants spanning the  
295 CC40.8 epitope and observed the presence of CC40.8-like epitope-targeting antibodies  
296 (Fig. 4B). The binding of cross-reactive serum Abs revealed dependence on five common  
297 stem helix residues including a conserved hydrophobic core formed by F<sup>1148</sup>, L<sup>1152</sup>, Y<sup>1155</sup>  
298 and F<sup>1156</sup> (Fig. 4B). To determine the contribution of S2-stem directed antibodies in overall  
299 SARS-CoV-2 neutralization by serum Abs in cross-reactive COVID-19 donors, we  
300 conducted competition experiments with the SARS-CoV-2 S2 stem-helix peptide. Peptide  
301 competition showed no or minimal effects on the SARS-CoV-2 neutralization (Fig. 4C and  
302 D), suggesting that stem-helix targeting cross-reactive nAbs minimally contribute to the  
303 overall polyclonal serum neutralization in these COVID-19 convalescent donors.

304

305

## 306 **Discussion**

307

308 The development of effective pan-coronavirus vaccine strategies that can mitigate future  
309 outbreaks from new emerging coronaviruses is important (16, 18). Two major challenges  
310 are the identification of broadly neutralizing antibody (bnAb) targets on CoV spike proteins  
311 and the development of vaccine strategies that can reproducibly elicit durable and  
312 protective pan-CoV bnAbs. The approach of identifying conserved bnAb surface protein  
313 targets by isolating bnAbs from natural infection and utilizing their molecular information  
314 in structure-guided immunogen design has greatly contributed to the development of  
315 vaccine strategies against a range of complex pathogen surfaces (63-70).

316

317 The spike S1 subunit shows considerable variation on HCoVs, whereas the S2 subunit is  
318 relatively more conserved, especially across the  $\beta$ -HCoVs, and appears to be promising  
319 for developing pan-CoV bnAb vaccine strategies. Accordingly, we recently isolated a  
320 SARS-CoV-1/2 cross-neutralizing Ab, CC40.8, that exhibits broad reactivity with human  
321  $\beta$ -CoVs (51). In this study, using epitope mapping and structural studies, we determined  
322 the spike epitope recognized by CC40.8. The epitope is located in the S2 stem-helix  
323 region, which is conserved across  $\beta$ -coronaviruses and may thus serve as a promising  
324 target for pan- $\beta$ -coronavirus vaccine strategies. The epitope is highly enriched in  
325 hydrophobic residues as well as some charged residues. The bnAbs targeting this region  
326 may neutralize by sterically interfering with the fusion machinery (52, 53), suggesting a  
327 potential target for fusion inhibitors (71-73). CC40.8 bnAb represents a human bnAb  
328 directed to the HCoV S2 stem helix (51). Two more S2 stem human bnAbs, S2P6 and

329 CV3-25, have also been reported recently (61, 74) that target a similar S2 stem epitope  
330 region. Knowledge from these nAbs will be important for developing broad vaccine  
331 strategies for  $\beta$ -coronaviruses.

332

333 We noted that cross-reactive antibodies directed to the CC40.8 S2 stem-helix epitope are  
334 much less frequently elicited in human coronavirus natural infections as compared to  
335 strain-specific neutralizing antibody responses (28). However, a few recent studies using  
336 more sensitive antibody detection assays have suggested a higher prevalence of  
337 polyclonal stem-helix region-directed antibodies in COVID-19 donors and their possible  
338 association with reduced disease severity (75-77). Regardless, the small subset of  
339 individuals in our sample cohort that do make cross-reactive Abs, seem to exhibit broad  
340 reactivity to human  $\beta$ -coronaviruses, which is promising for pan- $\beta$ -coronavirus vaccine  
341 strategies. In principle, the paucity of these cross-reactive antibodies could be due to poor  
342 accessibility of the S2 stem-helix epitope on the native spike protein relative to other  
343 epitopes, low frequency of bnAb-encoding B cell precursors in humans, or complex  
344 secondary B cell maturation pathways. Low epitope accessibility is clearly a potential  
345 contributor to low immunogenicity. Low precursor frequency seems unlikely, at least for  
346 CC40.8-like antibodies given that this antibody uses a common VH gene segment  
347 (IGHV3-23) and CDRH3 length (10 amino acids) (78). Analysis of CC40.8 antibody  
348 variable regions by the Armadillo tool (79) revealed the presence of several improbable  
349 somatic mutations that are predicted to contribute to difficulty in elicitation of CC40.8-like  
350 antibodies. Thus, isolation of multiple cross-reactive pan-CoV S2 stem bnAb lineages,  
351 understanding their maturation pathways, and identifying common antibody framework

352 motifs, are likely to be important for rational vaccine design approaches (80).  
353 Encouragingly, two recent studies have described a similar CoV S2 domain bnAb epitope  
354 being targeted by cross-reactive mAbs isolated from heterologous CoV spike protein  
355 immunizations in mice and mice transgenic for the human Ig locus (52, 53). These data  
356 suggest that such bnAbs could be induced by both immunization with designed vaccines  
357 as well as coronavirus infection in humans. Nonetheless, it would need to be ascertained  
358 how many sequential immunizations would be needed to broaden the breadth of these  
359 nAb responses.

360

361 Interestingly, despite relatively low neutralization potency, CC40.8 showed robust in vivo  
362 protective efficacy against SARS-CoV-2 challenge. The findings illustrate that extra-  
363 neutralizing effector functions of S2 stem bnAbs may be important and need to be  
364 investigated to determine their role in viral suppression or clearance. Indeed, recent  
365 studies have revealed that cross-reactive antibodies to endemic CoVs could serve as a  
366 marker for survival after severe disease (81, 82) or protection against COVID-19 (83).

367

368 Although we show CC40.8 S2 stem-helix bnAb confers in vivo protection against SARS-  
369 CoV-2 infection, our study has limitations. First, our CC40.8 protection studies were  
370 focused on SARS-CoV-2 infection and testing the protective efficacy of CC40.8 against  
371 a broad range of betacoronaviruses will be important. Second, we showed CC40.8  
372 protects against SARS-CoV-2 in two small animal models and investigating its protective  
373 efficacy in non-human primate models is also eventually desirable. Third, CC40.8 bnAb  
374 showed remarkable protection even at very low antibody levels despite its low

375 neutralization potency, hence warranting future studies to investigate the role of other  
376 factors such as antibody effector function that may contribute to CC40.8-mediated  
377 protection against coronaviruses.

378

379 Overall, we describe a cross-neutralizing human bnAb epitope on  $\beta$ -CoVs and provide  
380 molecular details that help explain its broad reactivity. The identification of this conserved  
381 epitope in the coronavirus spike protein should facilitate bnAb-epitope based vaccine  
382 development and antibody-based intervention strategies not only to SARS-CoV-2, but  
383 against existing human coronaviruses and other coronaviruses that could emerge with  
384 pandemic potential.

385

386

## 387 **Materials and Methods**

### 388 **Study Design**

389 The objective of the study was to evaluate a previously discovered SARS-CoV-2 spike  
390 protein stem-helix antibody, CC40.8, for binding to and neutralization of diverse  
391 sarbecoviruses and SARS-CoV-2 Variants of Concern, structurally define its epitope site  
392 and test its protective efficacy. For in vitro binding and neutralization studies, CC40.8 and  
393 control mAbs were tested in duplicate and experiments were repeated independently for  
394 rigor and reproducibility. We did not use any statistical methods to predetermine sample  
395 sizes for the animal studies. All hACE2-transgenic mouse or hamster experiments used 5  
396 or 6 animals per group. A positive and/or a negative control mAb-treated animal group  
397 was included in the in vivo SARS-CoV-2 challenge experiments. Male and female, age

398 matched (8-week old) animals were randomly assigned in CC40.8 bnAb-treated or control  
399 mAb-treated animal groups for the SARS-CoV-2 challenge studies. All immunological and  
400 virological measurements were performed blinded. Animals were euthanized at day five  
401 post infection to measure weight loss and lung viral load. The serum antibody titers of the  
402 passively transferred antibody were determined daily for the SARS-CoV-2 challenge  
403 experiment in the hACE2 mice. No datapoints were excluded as outliers in any  
404 experiment.

405

#### 406 **Human cohort information**

407 Plasma from convalescent COVID-19 donors were kindly provided through the “Collection  
408 of Biospecimens from Persons Under Investigation for 2019-Novel Coronavirus Infection  
409 to Understand Viral Shedding and Immune Response Study” UCSD IRB# 200236.  
410 Samples were collected based on COVID-19 diagnosis regardless of gender, race,  
411 ethnicity, disease severity, or other medical conditions. The gender for individuals was  
412 evenly distributed across the human cohort. All human donors were assessed for medical  
413 decision-making capacity using a standardized, approved assessment, and voluntarily  
414 gave informed consent prior to being enrolled in the study. The summary of the  
415 demographic information of the COVID-19 donors is listed in table S2.

416

#### 417 **Pseudovirus production and generation of mutant spike proteins**

418 Under biosafety level 2 and 3 conditions, MLV-gag/pol (Addgene #14887) and pCMV-  
419 Fluc (Addgene #170575) were co-transfected into HEK293T cells along with plasmids  
420 encoding full-length or variously truncated spike proteins from SARS-CoV-1, WIV1,

421 SHC014, PANG17, MERS-CoV and SARS-CoV-2 (SARS-CoV-2 variants of concern  
422 (B.1.1.7 (alpha), B.1.351 (beta), P.1 (gamma) and B.1.617.2 (delta)) using Lipofectamine  
423 2000 (Thermo Fisher Scientific cat.# 11668019) to produce single-round of infection  
424 competent pseudo-viruses. The media was changed by fresh Dulbecco's Modified Eagle  
425 Medium (DMEM) with 10% heat-inactivated FBS, 4mM L-Glutamine and 1% P/S 16 hours  
426 post transfection. The supernatant containing MLV-pseudotyped viral particles was  
427 collected 48 hours post transfection, aliquoted and frozen at -80 °C for the neutralization  
428 assay. Amino-acid point mutations in SARS-CoV-2 spike protein-encoding plasmids were  
429 made by using site-directed mutagenesis kit (New England Biolabs cat.# E0554S)  
430 according to the manufacturer's instructions. All the mutations were verified by DNA  
431 sequence analysis (Eton Bioscience).

432

### 433 **Neutralization assay**

434 Pseudotyped viral neutralization assay was performed as previously described with  
435 minor modifications (Modified from TZM-bl assay protocol (84)). In sterile 96-well half-  
436 area plates (Corning cat.# 3688), 25 µl of virus was immediately mixed with 25 µl of three-  
437 fold serially diluted monoclonal antibodies (mAb) (starting concentration of 300 µg/ml) or  
438 serially diluted plasma from COVID-19 donors and incubated for one hour at 37°C to allow  
439 for antibody neutralization of the pseudotyped virus. Synthesized peptides were optionally  
440 added in the mixture for testing inhibition of neutralization. 10,000 HeLa-hACE2 cells (as  
441 previously generated (33)) per well (in 50 µl of media containing 20 µg/ml Dextran) were  
442 directly added to the antibody virus mixture. Plates were incubated at 37°C for 42 to 48  
443 hours. Following the infection, HeLa-hACE2 cells were lysed using 1x luciferase lysis

444 buffer (25mM Gly-Gly pH 7.8, 15mM MgSO<sub>4</sub>, 4mM EGTA, 1% Triton X-100). Luciferase  
445 intensity was then read on a Luminometer with luciferase substrate according to the  
446 manufacturer's instructions (Promega cat.# E2620). Percentage of neutralization was  
447 calculated using the following equation:  $100 \times (1 - (\text{mean fluorescent intensity (MFI) of}$   
448  $\text{sample} - \text{average MFI of background}) / (\text{average of MFI of probe alone} - \text{average MFI of}$   
449  $\text{background}))$ . Fifty percent maximal inhibitory concentrations (IC<sub>50</sub>), the concentrations  
450 required to inhibit infection by 50% compared to the controls, were calculated using the  
451 dose-response-inhibition model with 5-parameter Hill slope equation in GraphPad Prism  
452 7 (GraphPad Software)

453

#### 454 **Flow cytometry based Cellular-ELISA (CELISA) binding**

455 Binding of monoclonal antibody to various human coronavirus (HCoV) spike proteins  
456 expressed on the surface of HEK293T cells was determined by flow cytometry, as  
457 described previously (85). Briefly, HEK293T cells were transfected with different plasmids  
458 encoding full-length HCoV spike proteins and were incubated for 36 to 48 hours at 37°C.  
459 Post incubation cells were trypsinized to prepare a single cell suspension and were  
460 distributed into 96-well plates. Monoclonal antibodies were prepared as 5-fold serial  
461 titrations in FACS buffer (1x phosphate-buffered saline (PBS), 2% fetal bovine serum  
462 (FBS), 1 mM EDTA), starting at 10 µg/ml, 6 dilutions. 50 µl/well of the diluted samples  
463 were added into the cells and incubated on ice for 1 hour. The plates were washed twice  
464 in FACS buffer and stained with 50 µl/well of 1:200 dilution of R-phycoerythrin (PE)-  
465 conjugated mouse anti-human IgG Fc antibody (SouthernBiotech cat.# 9040-09) and  
466 1:1000 dilution of Zombie-NIR viability dye (BioLegend cat.# 423105) on ice in dark for

467 45 minutes. After another two washes, stained cells were analyzed using flow cytometry  
468 (BD Lyric cytometers), and the binding data were generated by calculating the percent  
469 (%) PE-positive cells for antigen binding using FlowJo 10 software.

470

471 **Expression and purification of HCoV spike proteins and SARS-CoV-2 spike protein**  
472 **mutants**

473 To express the soluble spike ectodomain proteins, the HCoV spike protein encoding  
474 plasmids were transfected into FreeStyle293-F cells (Thermo Fisher Scientific cat.#  
475 R79007). For general production, 350 µg of plasmids were transfected into 1L  
476 FreeStyle293-F cells at the density of 1 million cells per mL. 350 µg plasmids in 16 ml  
477 Opti-MEM™ (Thermo Fisher Scientific cat.# 31985070 ) were filtered and mixed with 1.8  
478 mL 40K PEI (1mg/mL) in 16 ml Opti-MEM™. After gently mixing the two components, the  
479 combined solution rested at room temperature for 30 minutes and was poured into 1L  
480 FreeStyle293-F cell culture. The cell cultures were centrifuged at 2500xg for 15 minutes  
481 on day 4 after transfection, and the supernatants were filtered through the 0.22 µm  
482 membrane. The His-tagged proteins were purified with the HisPur Ni-NTA Resin (Thermo  
483 Fisher Scientific cat.# 88221). Each column was washed with at least 3 bed volumes of  
484 wash buffer (25 mM Imidazole, pH 7.4), followed by elution with 25 ml of the elution buffer  
485 (250 mM Imidazole, pH 7.4) at slow gravity speed (about 4 seconds per drop). The eluates  
486 were buffer exchanged into PBS by using Amicon tubes, and the proteins were  
487 concentrated afterwards. The proteins were further purified by size-exclusion  
488 chromatography using a Superdex 200 Increase 10/300 GL column (GE Healthcare cat.#

489 GE28-9909-44). The selected fractions were pooled and concentrated again for further  
490 use.

491

#### 492 **BioLayer Interferometry (BLI) binding**

493 The determination of monoclonal antibody binding with spike proteins or selected  
494 peptides was conducted in an Octet K2 system (ForteBio). The anti-human IgG Fc  
495 capture (AHC) biosensors (ForteBio cat.# 18-5063) were used to capture IgG first for 60  
496 seconds. After providing baseline in Octet buffer for another 60 seconds, the sensors  
497 were transferred into HCoV spike proteins at various concentrations for 120 seconds for  
498 association, and into Octet buffer for disassociation for 240 seconds. Alternatively, the  
499 hydrated streptavidin biosensors (ForteBio cat.# 18-5020) first captured the N-terminal  
500 biotinylated peptides diluted in Octet buffer (PBS plus 0.1% Tween-20) for 60 seconds,  
501 then transferred into Octet buffer for 60 seconds to remove unbound peptide and provide  
502 the baseline. Then the sensors were immersed in diluted monoclonal antibody IgG for  
503 120 seconds to provide association signal, followed by transferring into Octet buffer to  
504 test for disassociation signal for 240 seconds. The data generated was analyzed using  
505 the ForteBio Data Analysis software for correction, and the kinetic curves were fit to 1:1  
506 binding mode. Note that the IgG: spike protomer binding can be a mixed population of 2:1  
507 and 1:1, such that the term 'apparent affinity' dissociation constants ( $K_D^{App}$ ) are shown to  
508 reflect the binding affinity between IgGs and spike trimers tested.

509

#### 510 **HEp2 epithelial cell polyreactive assay**

511 Reactivity to human epithelial type 2 (HEp2) cells was determined by indirect  
512 immunofluorescence on HEp2 slides (Hemagen, cat.# 902360) according to  
513 manufacturer's instructions. Briefly, monoclonal antibody was diluted at 50  $\mu\text{g}/\text{mL}$  in PBS  
514 and then incubated onto immobilized HEp2 slides for 30 minutes at room temperature.  
515 After washing 3 times with PBS buffer, one drop of fluorescein isothiocyanate (FITC)-  
516 conjugated goat anti-human IgG was added onto each well and incubated in the dark for  
517 30 minutes at room temperature. After washing, the coverslip was added to HEp2 slide  
518 with glycerol and the slide was photographed on a Nikon fluorescence microscope to  
519 detect FITC signal.

520

#### 521 **Polyspecificity reagent (PSR) ELISA**

522 Solubilized CHO cell membrane protein (SMP) was coated onto 96-well half-area high-  
523 binding ELISA plates (Corning, cat.# 3690) overnight at 4°C. After washing with PBS plus  
524 0.05% Tween-20 (PBST), plates were blocked with 3% bovine serum albumin (BSA) for  
525 2 hours at 37°C. Antibody samples were diluted at 10  $\mu\text{g}/\text{mL}$  in 1% BSA with 3-fold serial  
526 dilution and then added in plates to incubate for 1 hour at 37°C. After 3 thorough washes  
527 with PBST, alkaline phosphatase-conjugated goat anti-human IgG Fc secondary antibody  
528 (Jackson ImmunoResearch, cat.# 109-055-008) was added to the plate and incubated  
529 for 1 hour at 37°C. After a final wash, phosphatase substrate (Sigma-Aldrich, cat.# S0942-  
530 200TAB) was added into each well. Absorption was measured at 405 nm.

531

#### 532 **Peptide scanning by ELISA binding**

533 N-terminal biotinylated overlapping peptides corresponding to the complete sequence of  
534 HCoV-HKU1 S2 subunit (residue number range: 761-1355 (GenBank: AAT98580.1) were  
535 synthesized at A&A Labs (Synthetic Biomolecules). Each peptide was 15 residue long  
536 with a 10 amino acid overlap. For ELISA binding, 96-well half-area plates (Corning cat. #  
537 3690) were coated overnight at 4°C with 2 µg/ml of streptavidin in PBS. Plates were  
538 washed 3 times with PBST and blocked with 3% (wt/vol) BSA in PBS for 1 hour. After  
539 removal of the blocking buffer, the plates were incubated with peptides in 1% BSA plus  
540 PBST for 1.5 hours at room temperature. After a washing step, monoclonal antibody or  
541 serum samples diluted in 1% BSA/PBST were added into each well and incubated for 1.5  
542 hours. DEN3 human antibody was used as a negative control. After the washes, a  
543 secondary antibody conjugated with alkaline phosphatase-conjugated goat anti-human  
544 IgG Fc secondary antibody (Jackson ImmunoResearch, cat.# 109-055-008) diluted  
545 1:1000 in 1% BSA/PBST, was added to each well and incubated for 1 hour. The plates  
546 were then washed and developed using alkaline phosphatase substrate pNPP tablets  
547 (Sigma-Aldrich, cat.# S0942-200TAB) dissolved in stain buffer. The absorbance was  
548 recorded at an optical density of 405 nm (OD405) using a VersaMax microplate reader  
549 (Molecular Devices), where data were collected using SoftMax software version 5.4.

550

### 551 **Cell-cell fusion inhibition assay**

552 HeLa stable cell lines were generated through transduction of lentivirus carrying genes  
553 encoding either human ACE2 (hACE2) and enhanced green fluorescent protein (EGFP)  
554 or nuclear localization signal (NLS)-mCherry and SARS-CoV-2 spike protein. The pBOB  
555 construct carrying these genes was co-transfected into HEK293T cells along with

556 lentiviral packaging plasmids pMDL, pREV, and pVSV-G (Addgene #12251, #12253,  
557 #8454) by Lipofectamine 2000 (Thermo Fisher Scientific, cat.# 11668019) according to  
558 the manufacturer's instructions. Supernatants were collected 48 hours after transfection,  
559 then were transduced to pre-seeded HeLa cells. 12 hours after transduction, stable cell  
560 lines were collected, scaled up and stored for cell-cell fusion assay. 10,000 NLS-  
561 mCherry<sup>+</sup> HeLa cells expressing SARS-COV-2 spike protein were seeded into 96-well  
562 half-well plates on the day before the assay. The culture medium was removed by  
563 aspiration before the assay. 50 µl of 50 µg/ml CC40.8 and DEN3 mAbs diluted in DMEM  
564 with 10% heat-inactivated FBS, 4mM L-Glutamine and 1% P/S were then added to the  
565 pre-seeded cells and incubated for 1 hour in an incubator. 50 µl of 10,000 EGFP<sup>+</sup>hACE2<sup>+</sup>  
566 HeLa cells were added to the plates and incubated for 2 hours before taking images under  
567 the microscope.

568

### 569 **Sequence alignments of coronavirus spike stem regions**

570 The spike sequences of SARS-CoV-2, SARS-CoV-1, RaTG13, SHC014, Rs4081,  
571 Pang17, RmYN02, Rf1, WIV1, Yun11, BM48-31, BtKY72, HCoV-HKU1, HCoV-OC43,  
572 MERS-CoV, MHV, HCoV-229E and HCoV-NL63 were downloaded from the GenBank  
573 and aligned against the SARS-CoV-2 reference sequence using BioEdit  
574 (<http://www.mbio.ncsu.edu/bioedit/bioedit.html>).

575

### 576 **Expression and purification of CC40.8 Fab**

577 To generate Fab, CC40.8 IgG was digested by Papain (Sigma-Aldrich cat.# P3125) for 4  
578 hours at 37 °C, then was incubated with Protein-A beads at 4 °C for 2 hours to remove

579 the Fc fragments. CC40.8 Fab was concentrated afterwards and further purified by size-  
580 exclusion chromatography using a Superdex 200 Increase 10/300 GL column (GE  
581 Healthcare cat.# GE28-9909-44). The selected fractions were pooled and concentrated  
582 again for further use.

583

#### 584 **Crystallization and structural determination**

585 A mixture of 9 mg/ml of CC40.8 Fab and 10× (molar ratio) SARS-CoV-2 stem peptide  
586 was screened for crystallization using the 384 conditions of the JCSG Core Suite (Qiagen)  
587 on our robotic CrystalMation system (Rigaku) at Scripps Research. Crystallization trials  
588 were set-up by the vapor diffusion method in sitting drops containing 0.1 µl of protein and  
589 0.1 µl of reservoir solution. Optimized crystals were then grown in drops containing 0.1 M  
590 sodium acetate buffer at pH 4.26, 0.2 M ammonium sulfate, and 28% (w/v) polyethylene  
591 glycol monomethyl ether 2000 at 20°C. Crystals appeared on day 7, were harvested on  
592 day 15 by soaking in reservoir solution supplemented with 20% (v/v) glycerol, and then  
593 flash cooled and stored in liquid nitrogen until data collection. Diffraction data were  
594 collected at cryogenic temperature (100 K) at Stanford Synchrotron Radiation Lightsource  
595 (SSRL) on the Scripps/Stanford beamline 12-1, with a beam wavelength of 0.97946 Å,  
596 and processed with HKL2000 (86). Structures were solved by molecular replacement  
597 using PHASER (87). A model of CC40.8 was generated by Repertoire Builder  
598 ([https://sysimm.ifrec.osaka-u.ac.jp/rep\\_builder/](https://sysimm.ifrec.osaka-u.ac.jp/rep_builder/)) (88). Iterative model building and  
599 refinement were carried out in COOT (89) and PHENIX (90), respectively. Epitope and  
600 paratope residues, as well as their interactions, were identified by accessing PISA at the  
601 European Bioinformatics Institute ([http://www.ebi.ac.uk/pdbe/prot\\_int/pistart.html](http://www.ebi.ac.uk/pdbe/prot_int/pistart.html)) (91).

602

### 603 **Animal Study**

604 8-week old transgenic hACE2 mice were given an i.p. antibody injections 12 hours pre-  
605 infection. Mice were infected through intranasal installation of  $2 \times 10^4$  total plaque-forming  
606 units (PFU) per animal of SARS-CoV-2 (USA-WA1/2020) in 25  $\mu$ L of DMEM. Mice were  
607 bled on days 1, 2, 3, and 5 for serum antibody detection and weighed for the duration of  
608 the study. At day 5 post-infection, animals were euthanized, and lungs were harvested  
609 for quantitative polymerase chain reaction (qPCR) viral titer analysis and plaque live virus  
610 analysis. Similar experimental procedures were conducted for the protection study in 8-  
611 week old Syrian hamsters except that a higher SARS-CoV-2 (USA-WA1/2020) challenge  
612 dose ( $10^6$  total PFU per animal) was used. The research protocol was approved and  
613 performed in accordance with Scripps Research IACUC Protocol #20-0003

614

### 615 **Antibody detection in hACE2 serum samples by ELISA**

616 Serum samples were obtained at day 1, 2, 3, and 5 to quantify mAb titers. Unconjugated  
617 F(ab')<sub>2</sub> fragment of goat anti-human F(ab')<sub>2</sub> fragment (Jackson ImmunoResearch cat.#  
618 109-006-097) was coated to the ELISA plates overnight, then washed by PBS plus 1%  
619 Tween-20 three times. After being blocked by 3% BSA for 2 hours at 37°C, mouse serum  
620 dilution series and CC40.8 mAb dilution series for a standard curve were applied to the  
621 plates and reacted for 1 hour at 37°C. After three thorough washes with PBS plus 1%  
622 Tween-20, alkaline phosphatase-conjugated goat anti-human IgG Fc secondary antibody  
623 (Jackson ImmunoResearch, cat.# 109-055-008) was added to the plates before washing

624 3 times with PBS plus 1% Tween-20 and AP substrate applied for detection. The plates  
625 were read at 405nm and data were analyzed by CurveExpert.

626

### 627 **SARS-CoV-2 RNA Quantification**

628 Viral RNA was isolated from lung tissue and subsequently amplified and quantified in a  
629 reverse transcription (RT)-qPCR reaction. Lung tissue was extracted at day 5 post  
630 infection and placed in 1 mL of trizol reagent (Invitrogen). The samples were then  
631 homogenized using a Bead Ruptor 12 (Omni International). Tissue homogenates were  
632 then spun down and the supernatant was added to an RNA purification column (Qiagen).  
633 Purified RNA was eluted in 60  $\mu$ L of DNase-, RNase-, endotoxin-free molecular biology  
634 grade water (Millipore). RNA was then subjected to reverse transcription and quantitative  
635 PCR using the CDC's N1 (nucleocapsid) primer sets (Forward 5'-GAC CCC AAA ATC  
636 AGC GAA AT-3'; Reverse 5'-TCT GGT TAC TGC CAG TTG AATCTG-3') and a  
637 fluorescently labeled (FAM) probe (5'-FAM-ACC CCG CAT TAC GTT TGGTGG ACC-  
638 BHQ1-3') (Integrated DNATechnologies) on a BioRad CFX96 Real-Time instrument. For  
639 quantification, a standard curve was generated by diluting  $2.5 \times 10^6$  PFU RNA equivalents  
640 of SARS-CoV-2. Every run utilized eleven 5-fold serial dilutions of the standard. SARS-  
641 CoV-2-negative mouse lung RNA and no templates were both included as negative  
642 controls for the extraction step as well as the qPCR reaction.

643

### 644 **Viral load measurements**

645 SARS-CoV-2 titers were measured by homogenizing organs in DMEM plus 2% fetal calf  
646 serum using 100  $\mu$ m cell strainers (Myriad cat.# 2825-8367). Homogenized organs were

647 titrated 1:10 over six steps and layered over Vero-E6 cells. After 1 hour of incubation at  
648 37°C, a 1% methylcellulose in DMEM overlay was added, and the cells were incubated  
649 for 3 days at 37°C. Cells were fixed with 4% paraformaldehyde and plaques were counted  
650 by crystal violet staining.

651

## 652 **Statistical Analysis**

653 Statistical analysis was performed using Graph Pad Prism 8 for Mac (Graph Pad  
654 Software). Groups of data were compared using the Kruskal-Wallis non-parametric test.  
655 Dunnett's multiple comparisons test were also performed between experimental groups.  
656 Data were considered statistically significant at  $p < 0.05$ .

657

## 658 **Supplementary Materials**

659 Fig S1 to S11

660 Table S1 and S2

661 Data File S1

662

## 663 References

- 664
- 665 1. C. Huang *et al.*, Clinical features of patients infected with 2019 novel coronavirus in  
666 Wuhan, China. *Lancet* **395**, 497-506 (2020).
- 667 2. Z. Wu, J. M. McGoogan, Characteristics of and Important Lessons From the Coronavirus  
668 Disease 2019 (COVID-19) Outbreak in China: Summary of a Report of 72314 Cases From  
669 the Chinese Center for Disease Control and Prevention. *JAMA*, (2020).
- 670 3. P. Zhou *et al.*, A pneumonia outbreak associated with a new coronavirus of probable bat  
671 origin. *Nature* **579**, 270-273 (2020).
- 672 4. J. Cui, F. Li, Z. L. Shi, Origin and evolution of pathogenic coronaviruses. *Nat Rev Microbiol*  
673 **17**, 181-192 (2019).
- 674 5. T. S. Fung, D. X. Liu, Human Coronavirus: Host-Pathogen Interaction. *Annu Rev Microbiol*  
675 **73**, 529-557 (2019).
- 676 6. C. Drosten *et al.*, Identification of a novel coronavirus in patients with severe acute  
677 respiratory syndrome. *The New England journal of medicine* **348**, 1967-1976 (2003).
- 678 7. A. M. Zaki, S. van Boheemen, T. M. Bestebroer, A. D. Osterhaus, R. A. Fouchier, Isolation  
679 of a novel coronavirus from a man with pneumonia in Saudi Arabia. *The New England*  
680 *journal of medicine* **367**, 1814-1820 (2012).
- 681 8. E. Petersen *et al.*, Comparing SARS-CoV-2 with SARS-CoV and influenza pandemics.  
682 *Lancet Infect Dis* **20**, e238-e244 (2020).
- 683 9. G. Meyerowitz-Katz, L. Merone, A systematic review and meta-analysis of published  
684 research data on COVID-19 infection fatality rates. *Int J Infect Dis* **101**, 138-148 (2020).
- 685 10. N. Wang *et al.*, Serological Evidence of Bat SARS-Related Coronavirus Infection in  
686 Humans, China. *Viol Sin* **33**, 104-107 (2018).
- 687 11. V. D. Menachery *et al.*, SARS-like WIV1-CoV poised for human emergence. *Proceedings*  
688 *of the National Academy of Sciences of the United States of America* **113**, 3048-3053  
689 (2016).
- 690 12. V. D. Menachery *et al.*, A SARS-like cluster of circulating bat coronaviruses shows  
691 potential for human emergence. *Nature medicine* **21**, 1508-1513 (2015).
- 692 13. M. Letko, A. Marzi, V. Munster, Functional assessment of cell entry and receptor usage  
693 for SARS-CoV-2 and other lineage B betacoronaviruses. *Nat Microbiol* **5**, 562-569 (2020).
- 694 14. S. J. Anthony *et al.*, Further Evidence for Bats as the Evolutionary Source of Middle East  
695 Respiratory Syndrome Coronavirus. *mBio* **8**, (2017).
- 696 15. X. Y. Ge *et al.*, Isolation and characterization of a bat SARS-like coronavirus that uses the  
697 ACE2 receptor. *Nature* **503**, 535-538 (2013).
- 698 16. D. R. Burton, E. J. Topol, Variant-proof vaccines - invest now for the next pandemic.  
699 *Nature* **590**, 386-388 (2021).
- 700 17. D. R. Burton, L. M. Walker, Rational Vaccine Design in the Time of COVID-19. *Cell host*  
701 *& microbe* **27**, 695-698 (2020).
- 702 18. W. C. Koff, S. F. Berkley, A universal coronavirus vaccine. *Science* **371**, 759 (2021).
- 703 19. J. R. Mascola, B. S. Graham, A. S. Fauci, SARS-CoV-2 Viral Variants-Tackling a Moving  
704 Target. *JAMA*, (2021).
- 705 20. P. Wang *et al.*, Antibody Resistance of SARS-CoV-2 Variants B.1.351 and B.1.1.7.  
706 *Nature*, (2021).
- 707 21. W. T. Harvey *et al.*, SARS-CoV-2 variants, spike mutations and immune escape. *Nat Rev*  
708 *Microbiol* **19**, 409-424 (2021).
- 709 22. C. K. Wibmer *et al.*, SARS-CoV-2 501Y.V2 escapes neutralization by South African  
710 COVID-19 donor plasma. *Nature medicine* **27**, 622-625 (2021).
- 711 23. F. Li, Structure, Function, and Evolution of Coronavirus Spike Proteins. *Annu Rev Virol* **3**,  
712 237-261 (2016).

- 713 24. F. Li, W. Li, M. Farzan, S. C. Harrison, Structure of SARS coronavirus spike receptor-  
714 binding domain complexed with receptor. *Science* **309**, 1864-1868 (2005).
- 715 25. A. C. Walls *et al.*, Structure, Function, and Antigenicity of the SARS-CoV-2 Spike  
716 Glycoprotein. *Cell* **181**, 281-292 e286 (2020).
- 717 26. D. Wrapp *et al.*, Cryo-EM structure of the 2019-nCoV spike in the prefusion conformation.  
718 *Science* **367**, 1260-1263 (2020).
- 719 27. H. Hofmann *et al.*, Human coronavirus NL63 employs the severe acute respiratory  
720 syndrome coronavirus receptor for cellular entry. *Proceedings of the National Academy of*  
721 *Sciences of the United States of America* **102**, 7988-7993 (2005).
- 722 28. L. Dai, G. F. Gao, Viral targets for vaccines against COVID-19. *Nature reviews.*  
723 *Immunology*, (2020).
- 724 29. F. Amanat, F. Krammer, SARS-CoV-2 Vaccines: Status Report. *Immunity* **52**, 583-589  
725 (2020).
- 726 30. F. Krammer, SARS-CoV-2 vaccines in development. *Nature* **586**, 516-527 (2020).
- 727 31. S. F. Ahmed, A. A. Quadeer, M. R. McKay, Preliminary Identification of Potential Vaccine  
728 Targets for the COVID-19 Coronavirus (SARS-CoV-2) Based on SARS-CoV  
729 Immunological Studies. *Viruses* **12**, (2020).
- 730 32. D. F. Robbiani *et al.*, Convergent antibody responses to SARS-CoV-2 in convalescent  
731 individuals. *Nature* **584**, 437-442 (2020).
- 732 33. T. F. Rogers *et al.*, Isolation of potent SARS-CoV-2 neutralizing antibodies and protection  
733 from disease in a small animal model. *Science* **369**, 956-963 (2020).
- 734 34. A. Z. Wec *et al.*, Broad neutralization of SARS-related viruses by human monoclonal  
735 antibodies. *Science* **369**, 731-736 (2020).
- 736 35. B. Ju *et al.*, Human neutralizing antibodies elicited by SARS-CoV-2 infection. *Nature* **584**,  
737 115-119 (2020).
- 738 36. R. Shi *et al.*, A human neutralizing antibody targets the receptor-binding site of SARS-  
739 CoV-2. *Nature* **584**, 120-124 (2020).
- 740 37. S. Du *et al.*, Structurally Resolved SARS-CoV-2 Antibody Shows High Efficacy in Severely  
741 Infected Hamsters and Provides a Potent Cocktail Pairing Strategy. *Cell* **183**, 1013-1023  
742 e1013 (2020).
- 743 38. S. J. Zost *et al.*, Potently neutralizing and protective human antibodies against SARS-  
744 CoV-2. *Nature* **584**, 443-449 (2020).
- 745 39. Y. Wu *et al.*, A noncompeting pair of human neutralizing antibodies block COVID-19 virus  
746 binding to its receptor ACE2. *Science* **368**, 1274-1278 (2020).
- 747 40. P. J. M. Brouwer *et al.*, Potent neutralizing antibodies from COVID-19 patients define  
748 multiple targets of vulnerability. *Science* **369**, 643-650 (2020).
- 749 41. J. Hansen *et al.*, Studies in humanized mice and convalescent humans yield a SARS-  
750 CoV-2 antibody cocktail. *Science* **369**, 1010-1014 (2020).
- 751 42. C. O. Barnes *et al.*, Structures of Human Antibodies Bound to SARS-CoV-2 Spike Reveal  
752 Common Epitopes and Recurrent Features of Antibodies. *Cell* **182**, 828-842 e816 (2020).
- 753 43. Y. Cao *et al.*, Potent Neutralizing Antibodies against SARS-CoV-2 Identified by High-  
754 Throughput Single-Cell Sequencing of Convalescent Patients' B Cells. *Cell* **182**, 73-84  
755 e16 (2020).
- 756 44. L. Premkumar *et al.*, The receptor binding domain of the viral spike protein is an  
757 immunodominant and highly specific target of antibodies in SARS-CoV-2 patients. *Sci*  
758 *Immunol* **5**, (2020).
- 759 45. M. Yuan *et al.*, Structural basis of a shared antibody response to SARS-CoV-2. *Science*  
760 **369**, 1119-1123 (2020).
- 761 46. Z. Wang *et al.*, mRNA vaccine-elicited antibodies to SARS-CoV-2 and circulating variants.  
762 *Nature* **592**, 616-622 (2021).

- 763 47. Y. Weisblum *et al.*, Escape from neutralizing antibodies by SARS-CoV-2 spike protein  
764 variants. *Elife* **9**, (2020).
- 765 48. E. Andreano *et al.*, SARS-CoV-2 escape from a highly neutralizing COVID-19  
766 convalescent plasma. *Proceedings of the National Academy of Sciences of the United*  
767 *States of America* **118**, (2021).
- 768 49. M. Yuan *et al.*, Structural and functional ramifications of antigenic drift in recent SARS-  
769 CoV-2 variants. *Science*, (2021).
- 770 50. K. Wu, W. Li, G. Peng, F. Li, Crystal structure of NL63 respiratory coronavirus receptor-  
771 binding domain complexed with its human receptor. *Proceedings of the National Academy*  
772 *of Sciences of the United States of America* **106**, 19970-19974 (2009).
- 773 51. G. Song *et al.*, Cross-reactive serum and memory B-cell responses to spike protein in  
774 SARS-CoV-2 and endemic coronavirus infection. *Nature communications* **12**, 2938  
775 (2021).
- 776 52. M. M. Sauer *et al.*, Structural basis for broad coronavirus neutralization. *Nature structural*  
777 *& molecular biology* **28**, 478-486 (2021).
- 778 53. C. Wang *et al.*, A conserved immunogenic and vulnerable site on the coronavirus spike  
779 protein delineated by cross-reactive monoclonal antibodies. *Nature communications* **12**,  
780 1715 (2021).
- 781 54. R. Andrabi *et al.*, Identification of Common Features in Prototype Broadly Neutralizing  
782 Antibodies to HIV Envelope V2 Apex to Facilitate Vaccine Design. *Immunity* **43**, 959-973  
783 (2015).
- 784 55. J. Jardine *et al.*, Rational HIV immunogen design to target specific germline B cell  
785 receptors. *Science* **340**, 711-716 (2013).
- 786 56. L. Cao *et al.*, Differential processing of HIV envelope glycans on the virus and soluble  
787 recombinant trimer. *Nature communications* **9**, 3693 (2018).
- 788 57. W. B. Struwe *et al.*, Site-Specific Glycosylation of Virion-Derived HIV-1 Env Is Mimicked  
789 by a Soluble Trimeric Immunogen. *Cell reports* **24**, 1958-1966 e1955 (2018).
- 790 58. J. Pallesen *et al.*, Immunogenicity and structures of a rationally designed prefusion MERS-  
791 CoV spike antigen. *Proceedings of the National Academy of Sciences of the United States*  
792 *of America* **114**, E7348-E7357 (2017).
- 793 59. C. L. Hsieh *et al.*, Structure-based design of prefusion-stabilized SARS-CoV-2 spikes.  
794 *Science* **369**, 1501-1505 (2020).
- 795 60. L. Bao *et al.*, The pathogenicity of SARS-CoV-2 in hACE2 transgenic mice. *Nature* **583**,  
796 830-833 (2020).
- 797 61. D. Pinto *et al.*, Broad betacoronavirus neutralization by a stem helix-specific human  
798 antibody. *Science* **373**, 1109-1116 (2021).
- 799 62. D. R. Burton, A new lease on life for an HIV-neutralizing antibody class and vaccine target.  
800 *Proceedings of the National Academy of Sciences of the United States of America* **118**,  
801 (2021).
- 802 63. D. R. Burton, Antibodies, viruses and vaccines. *Nature reviews. Immunology* **2**, 706-713  
803 (2002).
- 804 64. D. R. Burton, What Are the Most Powerful Immunogen Design Vaccine Strategies?  
805 Reverse Vaccinology 2.0 Shows Great Promise. *Cold Spring Harb Perspect Biol*, (2017).
- 806 65. S. F. Andrews, A. B. McDermott, Shaping a universally broad antibody response to  
807 influenza amidst a variable immunoglobulin landscape. *Curr Opin Immunol* **53**, 96-101  
808 (2018).
- 809 66. G. Barba-Spaeth *et al.*, Structural basis of potent Zika-dengue virus antibody cross-  
810 neutralization. *Nature* **536**, 48-53 (2016).
- 811 67. D. Corti, A. Lanzavecchia, Broadly neutralizing antiviral antibodies. *Annual review of*  
812 *immunology* **31**, 705-742 (2013).

- 813 68. C. Dreyfus *et al.*, Highly conserved protective epitopes on influenza B viruses. *Science*  
814 **337**, 1343-1348 (2012).
- 815 69. A. I. Flyak *et al.*, Broadly neutralizing antibodies from human survivors target a conserved  
816 site in the Ebola virus glycoprotein HR2-MPER region. *Nat Microbiol* **3**, 670-677 (2018).
- 817 70. B. S. Graham, M. S. A. Gilman, J. S. McLellan, Structure-Based Vaccine Antigen Design.  
818 *Annu Rev Med* **70**, 91-104 (2019).
- 819 71. F. Vigant, N. C. Santos, B. Lee, Broad-spectrum antivirals against viral fusion. *Nat Rev*  
820 *Microbiol* **13**, 426-437 (2015).
- 821 72. R. U. Kadam, I. A. Wilson, Structural basis of influenza virus fusion inhibition by the  
822 antiviral drug Arbidol. *Proceedings of the National Academy of Sciences of the United*  
823 *States of America* **114**, 206-214 (2017).
- 824 73. D. Eggink, B. Berkhout, R. W. Sanders, Inhibition of HIV-1 by fusion inhibitors. *Curr Pharm*  
825 *Des* **16**, 3716-3728 (2010).
- 826 74. N. K. Hurlburt *et al.*, Structural definition of a pan-sarbecovirus neutralizing epitope on the  
827 spike S2 subunit. *bioRxiv*, 2021.2008.2002.454829 (2021).
- 828 75. Y. Li *et al.*, Linear epitope landscape of the SARS-CoV-2 Spike protein constructed from  
829 1,051 COVID-19 patients. *Cell reports*, 108915 (2021).
- 830 76. Y. Li *et al.*, Linear epitopes of SARS-CoV-2 spike protein elicit neutralizing antibodies in  
831 COVID-19 patients. *Cell Mol Immunol* **17**, 1095-1097 (2020).
- 832 77. J. T. Ladner *et al.*, Epitope-resolved profiling of the SARS-CoV-2 antibody response  
833 identifies cross-reactivity with endemic human coronaviruses. *Cell Rep Med* **2**, 100189  
834 (2021).
- 835 78. B. Briney, A. Inderbitzin, C. Joyce, D. R. Burton, Commonality despite exceptional  
836 diversity in the baseline human antibody repertoire. *Nature* **566**, 393-397 (2019).
- 837 79. K. Wiehe *et al.*, Functional Relevance of Improbable Antibody Mutations for HIV Broadly  
838 Neutralizing Antibody Development. *Cell host & microbe* **23**, 759-765 e756 (2018).
- 839 80. R. Andrabi, J. N. Bhiman, D. R. Burton, Strategies for a multi-stage neutralizing antibody-  
840 based HIV vaccine. *Curr Opin Immunol* **53**, 143-151 (2018).
- 841 81. T. Zohar *et al.*, Compromised Humoral Functional Evolution Tracks with SARS-CoV-2  
842 Mortality. *Cell* **183**, 1508-1519 e1512 (2020).
- 843 82. U. Greenbaum *et al.*, High levels of common cold coronavirus antibodies in convalescent  
844 plasma are associated with improved survival in COVID-19 patients. *medRxiv*, (2021).
- 845 83. P. Kaplonek *et al.*, Early cross-coronavirus reactive signatures of humoral immunity  
846 against COVID-19. *Sci Immunol* **6**, eabj2901 (2021).
- 847 84. M. Sarzotti-Kelsoe *et al.*, Optimization and validation of the TZM-bl assay for standardized  
848 assessments of neutralizing antibodies against HIV-1. *Journal of immunological methods*  
849 **409**, 131-146 (2014).
- 850 85. L. M. Walker *et al.*, Broad and potent neutralizing antibodies from an African donor reveal  
851 a new HIV-1 vaccine target. *Science* **326**, 285-289 (2009).
- 852 86. Z. Otwinowski, W. Minor, Processing of X-ray diffraction data collected in oscillation mode.  
853 *Methods Enzymol* **276**, 307-326 (1997).
- 854 87. Afinogenov, II, [History of the pharmacy of the Main Hospital]. *Voen Med Zh* **318**, 57-60  
855 (1997).
- 856 88. D. Schmitt *et al.*, Repertoire Builder: high-throughput structural modeling of B and T cell  
857 receptors. *Molecular Systems Design & Engineering* **4**, 761-768 (2019).
- 858 89. P. Emsley, B. Lohkamp, W. G. Scott, K. Cowtan, Features and development of Coot. *Acta*  
859 *Crystallogr D Biol Crystallogr* **66**, 486-501 (2010).
- 860 90. P. D. Adams *et al.*, PHENIX: a comprehensive Python-based system for macromolecular  
861 structure solution. *Acta Crystallogr D Biol Crystallogr* **66**, 213-221 (2010).
- 862 91. E. Krissinel, K. Henrick, Inference of macromolecular assemblies from crystalline state.  
863 *Journal of molecular biology* **372**, 774-797 (2007).

- 864 92. S. Henikoff, J. G. Henikoff, Amino acid substitution matrices from protein blocks.  
865 *Proceedings of the National Academy of Sciences of the United States of America* **89**,  
866 10915-10919 (1992).
- 867 93. E. Jurrus *et al.*, Improvements to the APBS biomolecular solvation software suite. *Protein*  
868 *science : a publication of the Protein Society* **27**, 112-128 (2018).
- 869 94. T. J. Dolinsky, J. E. Nielsen, J. A. McCammon, N. A. Baker, PDB2PQR: an automated  
870 pipeline for the setup of Poisson-Boltzmann electrostatics calculations. *Nucleic acids*  
871 *research* **32**, W665-667 (2004).
- 872 95. J. Ye, N. Ma, T. L. Madden, J. M. Ostell, IgBLAST: an immunoglobulin variable domain  
873 sequence analysis tool. *Nucleic acids research* **41**, W34-40 (2013).
- 874 96. Y. Cai *et al.*, Distinct conformational states of SARS-CoV-2 spike protein. *Science* **369**,  
875 1586-1592 (2020).
- 876 97. D. Pinto *et al.*, Cross-neutralization of SARS-CoV-2 by a human monoclonal SARS-CoV  
877 antibody. *Nature* **583**, 290-295 (2020).
- 878 98. V. B. Chen *et al.*, MolProbity: all-atom structure validation for macromolecular  
879 crystallography. *Acta Crystallogr D Biol Crystallogr* **66**, 12-21 (2010).
- 880

881 **Acknowledgements**

882 We thank all of the human cohort participants for donating samples.

883

884 **Funding**

885 This work was supported by NIH NIAID CHAVD (UM1 AI44462 to D.R.B.), IAVI  
886 Neutralizing Antibody Center, the Bill and Melinda Gates Foundation (OPP 1170236 and  
887 INV-004923 to I.A.W. and D.R.B.), and the Translational Virology Core of the San Diego  
888 Center for AIDS Research (CFAR) AI036214. S.A.R. was supported by NIH  
889 5T32AI007384). This work was also supported by the John and Mary Tu Foundation and  
890 the James B. Pendleton Charitable Trust (to D.M.S. and D.R.B.). X-ray diffraction data  
891 were collected at Stanford Synchrotron Radiation Lightsource (SSRL). SSRL is a  
892 Directorate of SLAC National Accelerator Laboratory, and an Office of Science User  
893 Facility operated for the U.S. Department of Energy Office of Science by Stanford  
894 University. The SSRL Structural Molecular Biology Program is supported by the DOE  
895 Office of Biological and Environmental Research, and by the National Institutes of Health,  
896 National Institute of General Medical Sciences (including P41GM103393) and the  
897 National Center for Research Resources (P41RR001209).

898

899 **Author contributions**

900 P.Z., M.Y., G.S., I.A.W., D.R.B., and R.A. conceived and designed the study. N.B., J.R.,  
901 M.P., E.G., S.A.R., D.M.S., and T.F.R. recruited donors and collected and processed  
902 plasma samples. P.Z., G.S., and F.A., performed BLI, ELISA and cell binding and virus  
903 neutralization assays. D.H., and L.P., conducted cell-cell fusion experiment. W.H., S.C.,

904 and P.Y., generated recombinant protein antigens. M.Y. and X.Z. determined the crystal  
905 structure of the antibody-antigen complex. N.B., N.S., J.R.T., and T.F.R. carried out  
906 animal studies and viral load measurements. P.Z., M.Y., G.S., N.B., N.S., D.H., W.H.,  
907 D.N., J.R.T., T.F.R., I.A.W., D.R.B., and R.A. designed the experiments and analyzed the  
908 data. R.A., P.Z., G.S., M.Y., I.A.W. and D.R.B. wrote the paper, and all authors reviewed  
909 and edited the paper.

910

### 911 **Competing interests**

912 R.A., G.S., W.H., T.F.R., and D.R.B. are listed as inventors on pending patent  
913 applications describing the SARS-CoV-2 and HCoV-HKU1 S cross-reactive antibodies.  
914 P.Z., G.S., M.Y., I.A.W., D.R.B. and R.A. are listed as inventors on a pending patent  
915 application describing the S2 stem epitope immunogens identified in this study. All other  
916 authors have no competing interests to declare.

917

918 **Data Availability:** All data associated with this study are in the paper or supplementary  
919 materials.

920



936 are indicated.  $K_D^{App} < 10^{-12}M$  indicates that no off-rate could be measured. The raw  
937 experimental curves are shown as dash lines, while the solid lines are the fits.

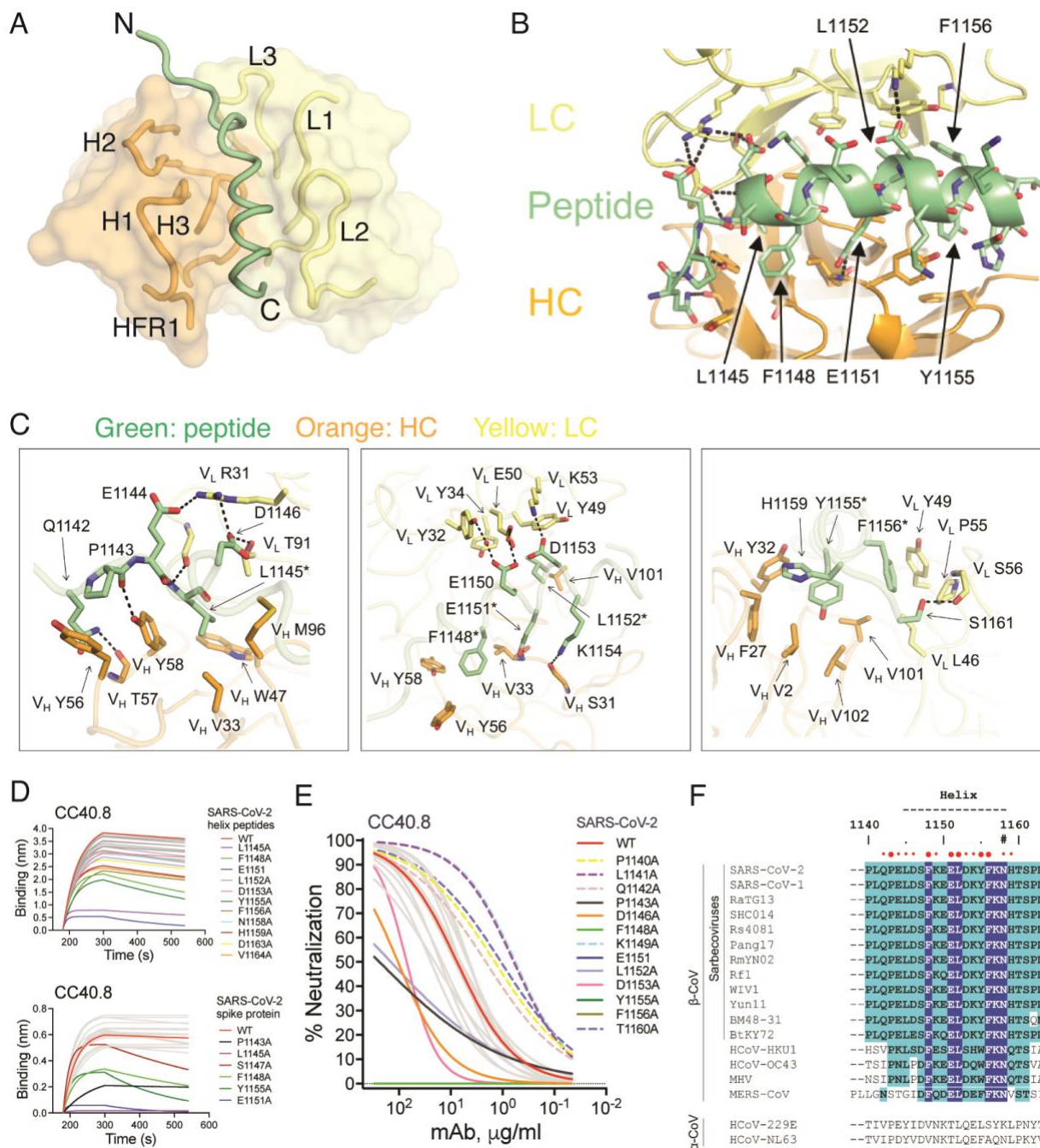
938 **(C)** Epitope mapping of CC40.8 with HCoV-HKU1 S2 subunit overlapping peptides is  
939 shown. A series of HCoV-HKU1 S2 (GenBank: AAT98580.1) overlapping biotinylated  
940 peptides (15-residues long with a 10-residue overlap) were tested for binding to CC40.8  
941 mAb by ELISA. OD405, optical density at 405nm. CC40.8 showed binding to the 95<sup>th</sup> 15-  
942 mer peptide corresponding to the HCoV-HKU1 S2 stem-helix region (residue position  
943 range: 1231-1245). An antibody to dengue virus, DEN3, was used as a control.

944 **(D)** BLI data are shown for CC40.8 binding to the HCoV-HKU1 95<sup>th</sup> 15-mer stem peptide  
945 (blue) and HCoV-HKU1 stem peptide variants with 5 additional residues either at the N-  
946 (20-mer: brick red) or C-(20-mer: orange) terminus or added at both termini (25-mer: red).  
947 CC40.8 showed strongest binding to the 25-residue stem peptide corresponding to  
948 HCoV-HKU1 S2 residues 1226-1250. The kinetic curves are fit with a 1:1 binding mode.

949 **(E)** BLI data are shown for CC40.8 binding to 25-mer stem peptides derived from different  
950 HCoV spikes. CC40.8 showed binding to the  $\beta$ - but not to the  $\alpha$ -HCoV S2 stem peptides.  
951 The HCoV-HKU1 S2 residues 1226-1250 correspond to residues 1140-1164 on SARS-  
952 CoV-2 spike. The kinetic curves are fit with a 1:1 binding mode.

953 **(F)** A SARS-CoV-2 spike protein cartoon depicts the S2-stem epitope region in green at  
954 the base of the prefusion spike ectodomain.

955 **(G)** Sequence conservation of the CC40.8 stem-helix epitope is shown for SARS-CoV-  
956 1/2, HCoV-HKU1 and HCoV-OC43 human  $\beta$ -CoV spike proteins. Conserved identical  
957 residues are highlighted with blue boxes, and similar residues are in cyan boxes [amino  
958 acids scored greater than or equal to 0 in the BLOSUM62 alignment score matrix (92)  
959 were counted as similar here]. An N-linked glycosylation site is indicated with a “#”  
960 symbol.  
961



962  
 963 **Figure 2. Crystal structure of CC40.8 antibody in complex with the SARS-CoV-2**  
 964 **stem peptide, and S2 stem bnAb epitope residues and conservation across CoVs.**  
 965 **(A)** An overall view of the CC40.8-peptide complex structure is shown at 1.6 Å resolution.  
 966 Heavy and light chains of CC40.8 are shown in orange and yellow semi-transparent  
 967 surfaces, respectively, with the heavy (H) and light (L) chain complementary determining  
 968 regions (CDRs) shown as tubes. The SARS-CoV-2 stem-helix peptide is shown as a  
 969 green tube for the peptide backbone.  
 970 **(B)** An overview of the CC40.8 antibody and S2 stem-peptide interaction is shown. Heavy  
 971 (H) and light (L) chains of CC40.8 are shown in orange and yellow, respectively, whereas

972 the SARS-CoV-2 stem peptide is in green. Hydrogen bonds and salt bridges are  
973 represented by black dashed lines.

974 **(C)** Details of the interactions between CC40.8 and the SARS-CoV-2 stem peptide are  
975 shown. Residues conserved in SARS-CoV-1, SARS-CoV-2, and other sarbecoviruses as  
976 well as seasonal  $\beta$ -CoVs HCoV-HKU-1, and HCoV-OC43 are labeled with asterisks (\*).

977 **(D)** BLI data are shown for binding of CC40.8 bnAb to SARS-CoV-2 stem-helix peptide  
978 (top) and soluble spike protein alanine mutants (bottom) spanning the whole epitope. The  
979 stem peptide or spike protein mutants that substantially affect CC40.8 bnAb binding are  
980 shown in assorted colors in comparison to wild-type (WT, red).

981 **(E)** Neutralization of SARS-CoV-2 and the stem-helix alanine mutants spanning the whole  
982 epitope by CC40.8 is shown. The WT virus is shown in red and virus mutants that  
983 substantially affect CC40.8 bnAb neutralization are shown in assorted colors. The bold  
984 and dashed color curves indicate substitutions that, respectively, led to a decrease or an  
985 increase in the  $IC_{50}$  neutralization titers compared to WT virus.

986 **(F)** Sequence conservation is shown for the CC40.8 stem-helix epitope on SARS-CoV-  
987 1/2, sarbecoviruses infecting other animal species, human  $\beta$ -CoVs and mouse hepatitis  
988 virus (MHV). The stem region forming the helix is indicated by black dashes and residues  
989 involved in interaction with CC40.8 antibody are indicated by red dots (cutoff distance =  
990 4 Å). Larger dots indicate residues that are essential for CC40.8 interaction as defined by  
991 alanine scanning mutagenesis where mutation decreased neutralization  $IC_{50}$  by at least  
992 10-fold or a complete knock-out (details are shown in fig. S7). Conserved identical  
993 residues are highlighted with blue boxes, and similar residues are in cyan boxes [amino  
994 acids scored greater than or equal to 0 in the BLOSUM62 alignment score matrix (92)  
995 were counted as similar here]. An N-linked glycosylation site is indicated with a “#”  
996 symbol. The region that presents a helical secondary structure in the CC40.8/peptide  
997 structure is indicated on top of the panel.

998

999

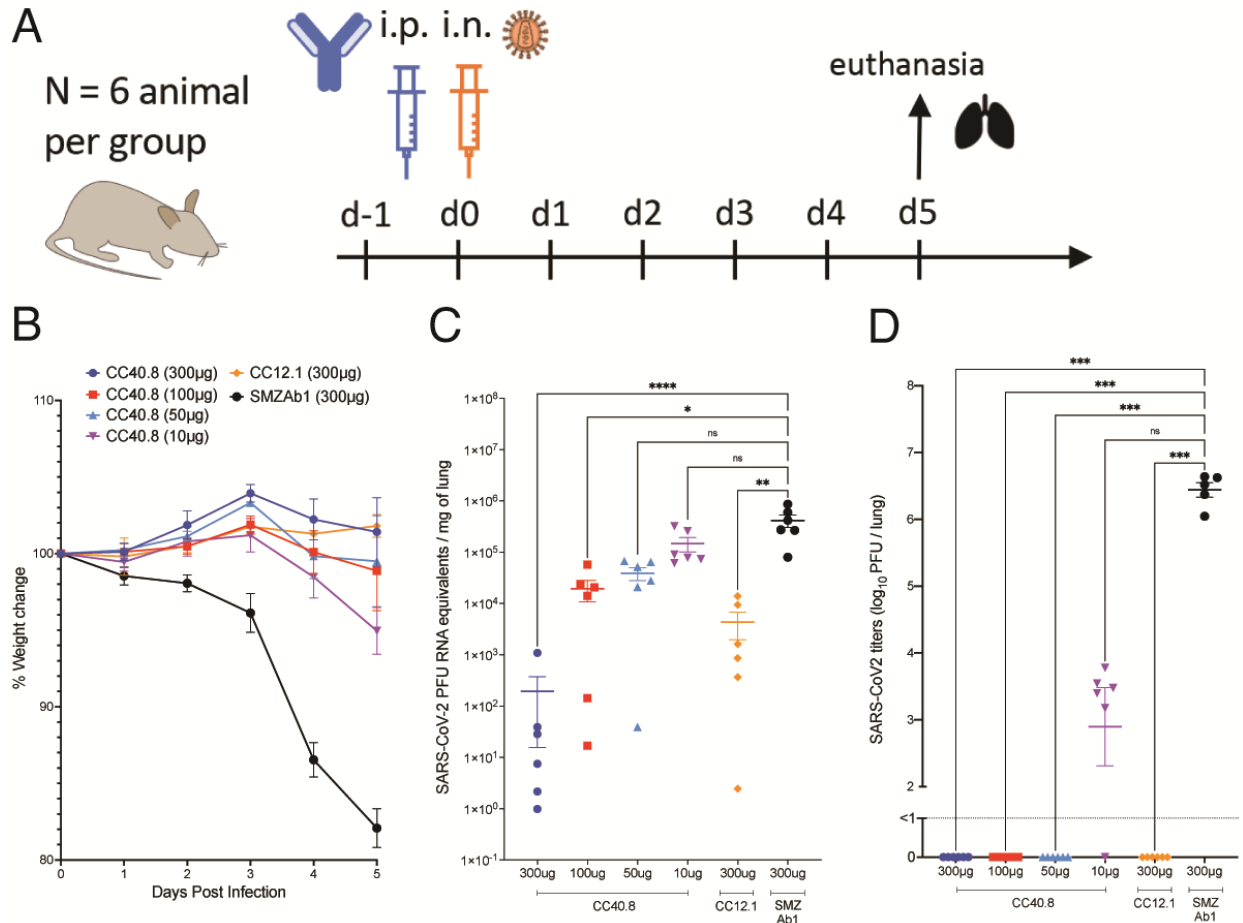


**Figure 3. CC40.8 reduces weight loss, lung viral load, and viral replication following SARS-CoV-2 challenge in the hACE2 mouse model.**

**(A)** CC40.8 was administered intraperitoneally (i.p.) at four different doses (300 µg, 100 µg, 50 µg, and 10 µg) per animal into hACE2 receptor-expressing mice (6 animals per group). Control animals received CC12.1 RBD nAb (300 µg per animal) or a Zika-specific mAb, SMZAb1 (300 µg per animal). Each group of animals was challenged intranasally (i.n.) 12 hours after antibody infusion with  $2 \times 10^4$  PFU of SARS-CoV-2 (USA-WA1/2020). Animal weight was monitored daily as an indicator of disease progression and lung tissue was collected on day 5 for viral load and viral burden assessment.

**(B)** Percent weight change in CC40.8 or control antibody-treated animals after SARS-CoV-2 challenge is shown. Percent weight change was calculated from day 0 for all animals. Data are presented as mean  $\pm$  SEM.

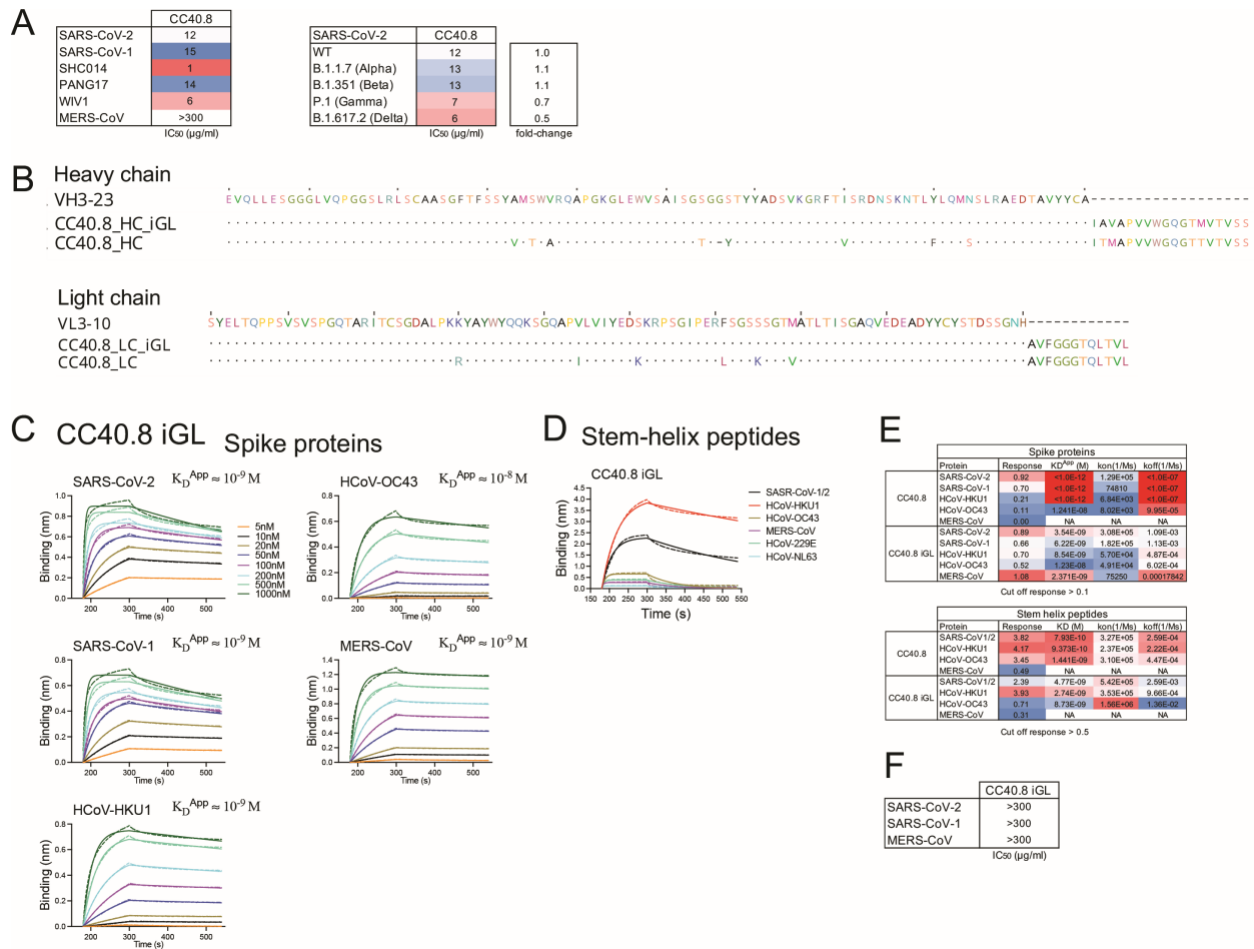
**(C)** SARS-CoV-2 viral RNA loads based on the qPCR analysis of lung tissue at day 5 after infection are shown. Data are presented as mean  $\pm$  SEM.

**(D)** SARS-CoV-2 infectious virus titers (plaque-forming unit (PFU)) are shown as determined by plaque assay from lung tissue at day 5 after infection. Data are presented as mean  $\pm$  SEM.

Statistical comparisons between groups were performed using a Kruskal-Wallis non-parametric test followed by Dunnett's multiple comparisons. (\*p <0.05, \*\*p <0.01, \*\*\*p <0.001; \*\*\*\*p < 0.0001; ns, p >0.05).



1054 **SUPPLEMENTARY MATERIALS**  
1055



1056

1057

1058

1059

1060

1061

1062

1063

1064

1065

1066

1067

1068

1069

1070

1071

1072

1073

1074

1075

1076

1077

**Fig. S1. CC40.8 mature and CC40.8 iGL antibodies bind to spike proteins and stem-helix peptides and mature antibody neutralizes pseudotyped coronaviruses.**

**(A)** IC<sub>50</sub> neutralization of CC40.8 broadly neutralizing antibody (bnAb) is shown for sarbecoviruses (SARS-CoV-2, SARS-CoV-1, SHC014, Pang17 and WIV1), MERS-CoV and SARS-CoV-2 variants of concern (alpha (B.1.1.7), beta (B.1.351), gamma (P.1) and delta (B.1.617.2)).

**(B)** Sequence alignment of CC40.8 heavy and light chains with their corresponding germline V-gene sequences (VH3-23 and VL3-10) is shown with the design of CC40.8 antibody inferred germline (iGL) gene sequences. Dots represent identical residues and dashes represent gaps introduced to preserve the alignment.

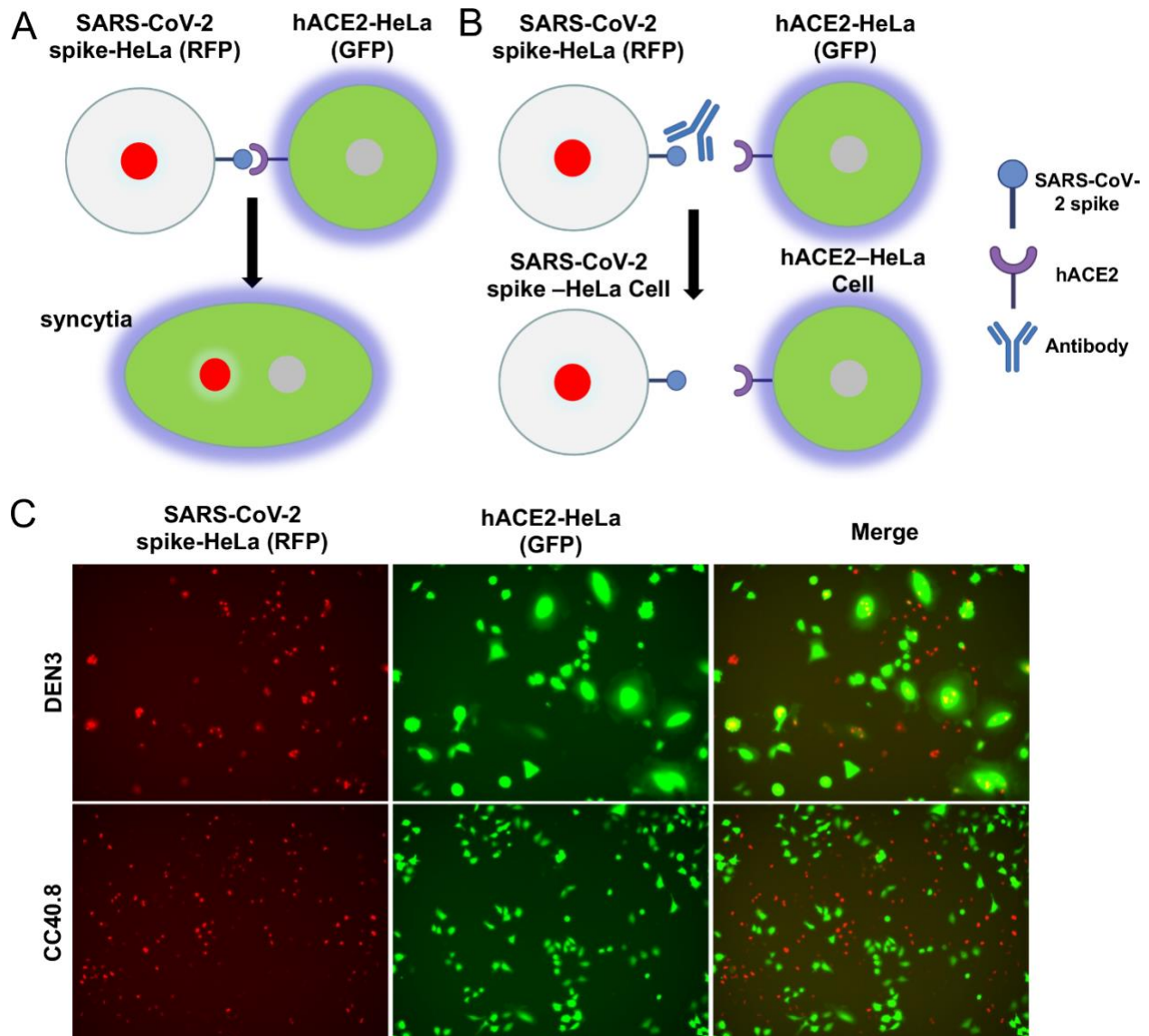
**(C)** BioLayer Interferometry (BLI) binding is shown for CC40.8 iGL antibody with human β-HCoV soluble spike proteins. Apparent binding constants (K<sub>D</sub><sup>APP</sup>) for each antibody-antigen interaction are indicated. The raw experimental curves are shown as dash lines, while the solid lines are the fits.

**(D)** BLI binding is shown for CC40.8 iGL Ab to 25-mer stem peptides derived from all HCoV spike proteins. The kinetic curves are fit with a 1:1 binding mode.

**(E)** Binding kinetics (K<sub>D</sub><sup>APP</sup> (spike proteins), K<sub>D</sub> (stem-helix peptides) k<sub>on</sub> and k<sub>off</sub> constants) of CC40.8 and CC40.8 iGL antibodies with human β-HCoV soluble spike proteins and the 25-mer β-HCoV stem peptides are shown.

**(F)** IC<sub>50</sub> neutralization of CC40.8 iGL is shown for sarbecoviruses (SARS-CoV-2 and SARS-CoV-1) and MERS-CoV.

1078



1079

1080

1081

1082

1083

1084

1085

1086

1087

1088

1089

1090

1091

1092

1093

**Fig. S2. CC40.8 antibody inhibits SARS-CoV-2 spike protein- and hACE2-mediated cell-cell fusion.**

**(A and B)** A schematic diagram of cell-cell fusion assay is shown. SARS-CoV-2 spike-HeLa cells express nucleus-restricted RFP (Red) and hACE2-HeLa cells express cytosolic GFP (Green). The interaction of SARS-CoV-2 spike protein and hACE2 can lead to cell fusion to form syncytia. In the same syncytium, both GFP in the cytoplasm and RFP in the nucleus can be seen (A). If antibody can block cell-cell fusion, no syncytia can be seen. Only GFP-expressing hACE2-HeLa cells and RFP-expressing SARS-CoV-2 spike-HeLa cells can be seen (B).

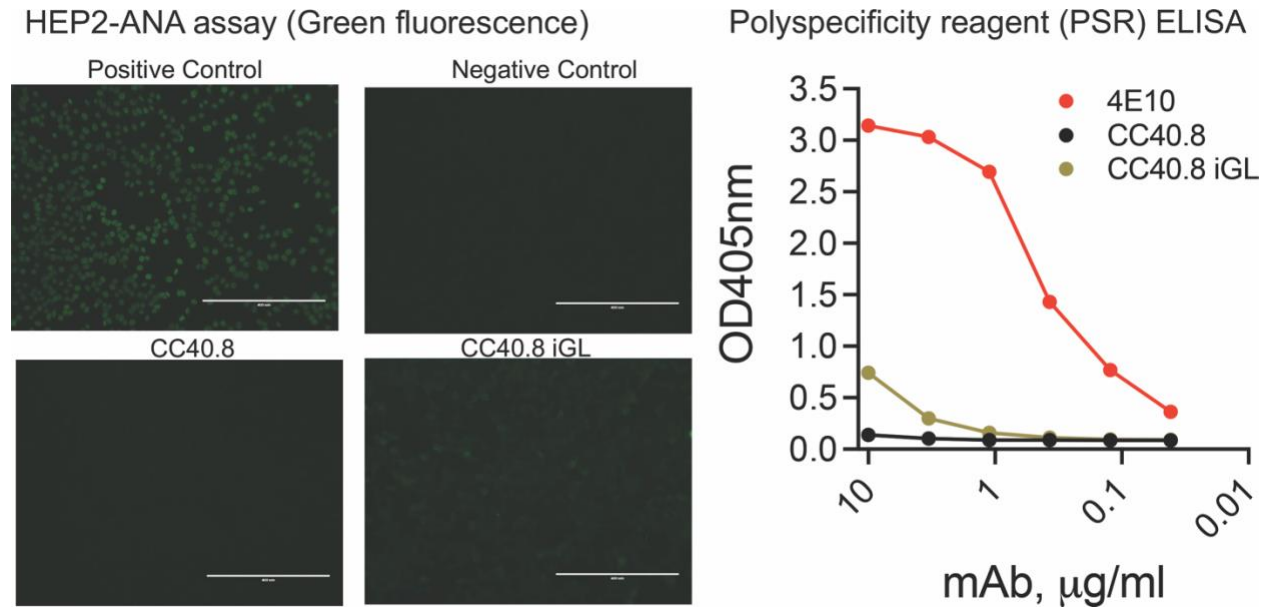
**(C)** SARS-CoV-2 spike-HeLa cells (red) were pre-incubated with negative control antibody (DEN3) or CC40.8 S2 stem bnAb for 1 hour, and then mixed with hACE2-HeLa cells (green). Green syncytia were observed with DEN3, indicating widespread cell-cell fusion mediated by SARS-CoV-2 spike and hACE2; fusion was inhibited by addition of CC40.8.

Peptide number	HKU1 S2 residues	Sequence	OD405nm		Peptide number	HKU1 S2 residues	Sequence	OD405nm		Peptide number	HKU1 S2 residues	Sequence	OD405nm	
			CC40.8	DEN3				CC40.8	DEN3				CC40.8	DEN3
1	761-775	SISASYRFVTFEFPN	0.2	0.2	40	956-970	ESQISGYTTAATVAA	0.1	0.2	79	1151-1165	SYKPISFKTVLVSPG	0.2	0.2
2	766-780	YRFVTFEFPNVSVFN	0.2	0.2	41	961-975	GYTTAATVAAMFPFW	0.2	0.2	80	1156-1170	SFKTVLVSPGLCISG	0.2	0.3
3	771-785	FEFNVSVFVNDISIES	0.1	0.2	42	966-980	ATVAAMFPFWSAAG	0.1	0.2	81	1161-1175	LVSPLGLCISGDVGLA	0.2	0.2
4	776-790	VSVFVNDISIEVSGGLY	0.1	0.2	43	971-985	MFPFWSAAGIPFSL	0.2	0.2	82	1166-1180	LCISGDVGIAPVQGY	0.2	0.2
5	781-795	DSIESVGGLYEIKIP	0.2	0.2	44	976-990	SAAAGIPFSLVQYR	0.2	0.2	83	1171-1185	DVGIAPQGYFKIHN	0.2	0.2
6	786-800	VGGLYEIKIPYPTFTI	0.1	0.2	45	981-995	IPFSLVQYRINGLG	0.2	0.2	84	1176-1190	PKQGYFKIHNHWMF	0.2	0.2
7	791-805	EIKIPYPTFTIVGQEE	0.1	0.2	46	986-1000	NVQYRINGLGVTMDV	0.2	0.2	85	1181-1195	FKIHNHWMFTGSSY	0.2	0.3
8	796-810	TNFTIVGQEEFIQTN	0.1	0.2	47	991-1005	INGLGVMTDVLNKNQ	0.1	0.2	86	1186-1200	DHWMFTGSSYYPFP	0.2	0.2
9	801-815	VQGEEFIQTNSPKVT	0.1	0.2	48	996-1010	VMTDVLNKNQKLIAT	0.2	0.2	87	1191-1205	TGSSYYPFPISDKN	0.2	0.2
10	806-820	FIQTNSPKVTIDCSL	0.2	0.2	49	1001-1015	LKNQKLIATAFNNA	0.2	0.2	88	1196-1210	YFPISDKNVVFMN	0.2	0.2
11	811-825	SPKVTIDCSLDFVCSN	0.2	0.2	50	1006-1020	KLIATAFNNAISIQ	0.2	0.2	89	1201-1215	ISDKNVVFMNVCVFN	0.2	0.2
12	816-830	IDCSLDFVCSNYAACH	0.2	0.2	51	1011-1025	AFNNAISIQNGFSA	0.2	0.2	90	1206-1220	VFMNVCVFNFTKAP	0.2	0.2
13	821-835	FVCSNYAACHDLLSE	0.2	0.3	52	1016-1030	LLSQNGFSATNSAL	0.1	0.2	91	1211-1225	TCSVNFTRKAPLYLN	0.2	0.3
14	826-840	YAACHDLLSEYGTFC	0.2	0.3	53	1021-1035	NGFSATNSALAIQIS	0.2	0.2	92	1216-1230	FTKAPLYLNHNSVFK	0.2	0.2
15	831-845	DLLSEYGTFCNDINS	0.2	0.3	54	1026-1040	TNSALAIQSVVNSN	0.2	0.2	93	1221-1235	LVLYLNHNSVFKLSDFE	0.2	0.2
16	836-850	YGTFCNDINSILDEV	0.2	0.2	55	1031-1045	AKIQSVVNSNAQALN	0.2	0.2	94	1226-1240	HSVPKLSDFESELHSH	0.2	0.2
17	841-855	DNINSILDEVNGLLD	0.1	0.2	56	1036-1050	VVNSNAQALNSLLQQ	0.2	0.2	95	1231-1245	LSDFESELHSHWFKQ	2.5	0.2
18	846-860	ILDEVNGLLDTTQLH	0.1	0.2	57	1041-1055	AQALNSLLQQLEFKF	0.2	0.3	96	1236-1250	SELHSHWFKQTSIAF	0.2	0.2
19	851-865	NGLLDTTQLHVAADTL	0.1	0.2	58	1046-1060	SLLDLQLEFKFSAISS	0.2	0.2	97	1241-1255	WFKQTSIAFNLTLLN	0.2	0.2
20	856-870	TTQLHVAADTLMQGVT	0.1	0.2	59	1051-1065	LFNKFSALSSSLQEI	0.2	0.2	98	1246-1260	TSIAFNLTLLNLTIN	0.2	0.2
21	861-875	VADTLMQGVTLSNLSNL	0.1	0.2	60	1056-1070	GAISSSLQELSLRLD	0.2	0.2	99	1251-1265	NLTLLNLTINATFFLD	0.2	0.2
22	866-880	MQGVTLSNLSNLTNLH	0.1	0.2	61	1061-1075	SLQELSLRLDALENAQ	0.2	0.3	100	1256-1270	LHTINATFLDLYEM	0.2	0.2
23	871-885	LSSNLTNLHFPVDN	0.1	0.2	62	1066-1080	LSRLDALENAQVQIDR	0.2	0.2	101	1261-1275	ATFLDLYEMNLIQE	0.2	0.2
24	876-890	NTNLHFPVDNINFKS	0.1	0.2	63	1071-1085	ALENAQVQIDRLNRLG	0.2	0.2	102	1266-1280	LYEMNLIQESIKSL	0.2	0.2
25	881-895	FVDNINFKSLVGLCL	0.2	0.3	64	1076-1090	VQIDRLNRLTALN	0.2	0.2	103	1271-1285	NLIQESIKSLNNSYI	0.2	0.2
26	886-900	INFKSLVGLGPHCG	0.2	0.3	65	1081-1095	LINGRLTALNAVVSQ	0.2	0.2	104	1276-1290	SIKSLNNSYINLKI	0.2	0.2
27	891-905	LVGLGPHCGSSRS	0.2	0.2	66	1086-1100	LTALNAVVSQQLSDI	0.2	0.3	105	1281-1295	NNSYINLKDITGYEM	0.2	0.2
28	896-910	GPHCGSSRSFFEDL	0.2	0.2	67	1091-1105	AVVSQQLSDISLVKF	0.2	0.3	106	1286-1300	NLKDITGYEMVYKVP	0.2	0.2
29	901-915	SSRSFFEDLDFPKV	0.2	0.2	68	1096-1110	QLSDISLVKFGAALA	0.2	0.2	107	1291-1305	GYEMVYKVPVWNL	0.3	0.3
30	906-920	FFEDLDFKVKLSVDV	0.1	0.2	69	1101-1115	SLVKFGAALAMEKVN	0.2	0.2	108	1296-1310	YVWVWVWVWVWVWV	0.3	0.2
31	911-925	LFDKVKLSVDFGVEA	0.2	0.2	70	1106-1120	GAALAMEKVNCEVKS	0.2	0.2	109	1301-1315	WVWVWVWVWVWVWV	0.2	0.2
32	916-930	KLSVDFGVEAYNNTC	0.2	0.3	71	1111-1125	MEKVNCEVKSQSPRI	0.2	0.3	110	1306-1320	LISFSLIFSLVLIFF	0.1	0.2
33	921-935	GFVEAYNNTCGGSEI	0.2	0.2	72	1116-1130	ECVKSQSPRINFCGN	0.2	0.2	111	1311-1325	FISFLVLIFFICCT	0.2	0.2
34	926-940	YNNCTGGSEIRDLLC	0.2	0.2	73	1121-1135	QSPRINFCGNHHL	0.2	0.2	112	1316-1330	VLIFFICCTGGCGSA	0.2	0.3
35	931-945	GGSEIRDLLCVQSFN	0.2	0.2	74	1126-1140	NFCGNHHLISLVQN	0.2	0.2	113	1321-1335	ICCTGGCGSACFSKC	0.2	0.3
36	936-950	RDLLCVQSFNGIKVFL	0.2	0.2	75	1131-1145	GNHHLISLVQNPYGL	0.2	0.2	114	1326-1340	CGGSACFSKCHNCDC	0.2	0.3
37	941-955	VQSFNGIKVFLPPLS	0.2	0.2	76	1136-1150	SLVQNPYGLLFMHF	0.2	0.3	115	1331-1345	CFSKCHNCDEYGGH	0.2	0.2
38	946-960	GKVLFPPLSSEIQIS	0.2	0.2	77	1141-1155	APYGLLFMHFYSKPI	0.2	0.3	116	1336-1350	HNCDEYGGHHDFVI	0.2	0.3
39	951-965	FPPLSSEIQISGYTTA	0.2	0.2	78	1146-1160	LFMHFYSKPISEKTV	0.2	0.2	117	1341-1355	EYGGHDFVIKTSHD	0.2	0.2

**Fig. S3. Epitope mapping of CC40.8 antibody with HCoV-HKU1 S2 subunit-derived overlapping peptides.**

ELISA binding results are shown for CC40.8 mAb with HCoV-HKU1 S2 subunit overlapping peptides (residue number range: 761-1355). Each HCoV-HKU1 S2 subunit peptide is 15-residues long with a 10-residue overlap. Peptide IDs, S2 subunit residue number ranges of 15-mer peptides, and antibody binding responses are shown. CC40.8 exhibited binding to the 95<sup>th</sup> peptide (residue position range: 1231-1245) corresponding to the HCoV-HKU1 S2 stem-helix region. DEN3, an antibody to dengue virus, was used as a control.

1094  
1095  
1096  
1097  
1098  
1099  
1100  
1101  
1102  
1103  
1104

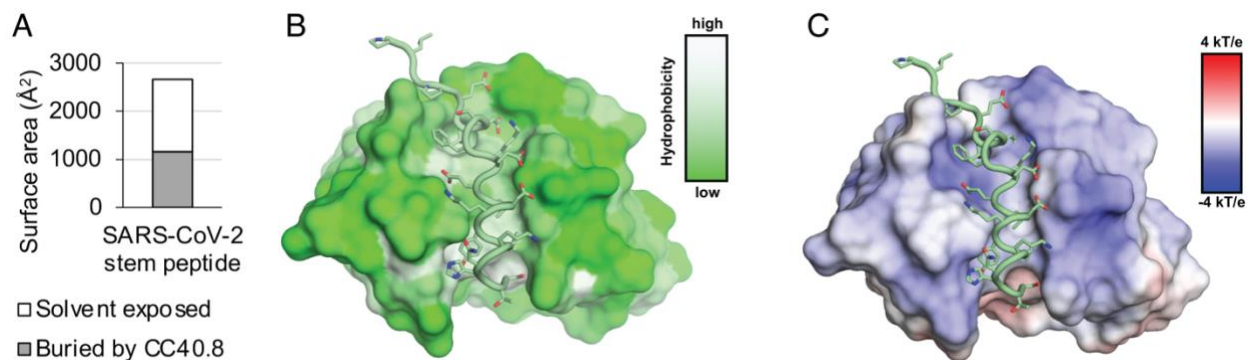


1105  
1106  
1107  
1108  
1109  
1110  
1111  
1112  
1113  
1114

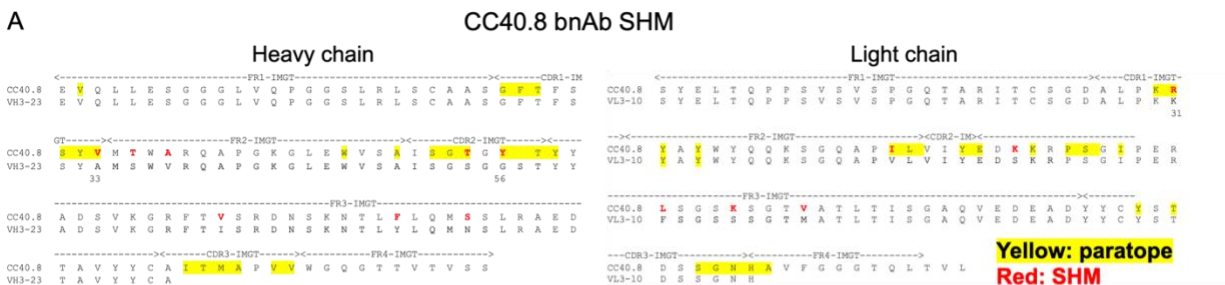
**Fig. S4. Polyreactivity analysis of CC40.8 and CC40.8 iGL antibodies.**

**(A)** Immunofluorescence showing binding of antibodies to immobilized HEP2 epithelial cells was detected by FITC-labelled secondary antibody. Positive and negative controls for the Hep2 kit assay are provided by the manufacturer.

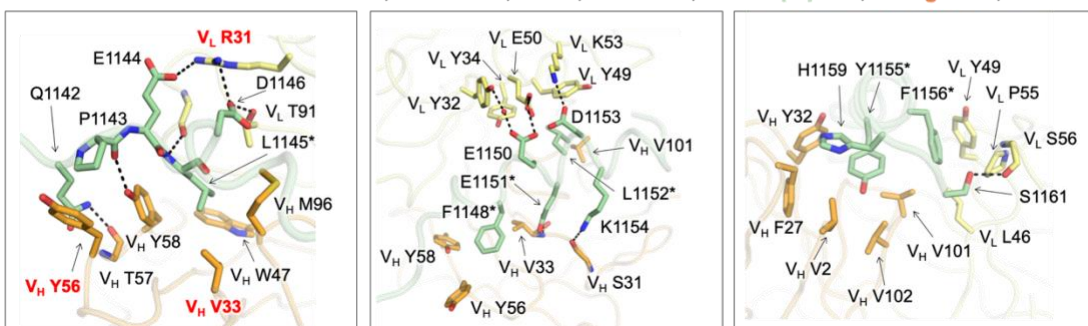
**(B)** Antibodies were tested by enzyme-linked immunosorbent assay (ELISA) for binding to the polyspecificity reagent (PSR) from CHO-cell solubilized membrane protein (SMP). 4E10, an HIV MPER-specific antibody known to display polyreactivity, was used as a positive control.



1115  
1116 **Fig. S5. CC40.8 bnAb structure with SARS-CoV-2 S2 stem-helix peptide.**  
1117 **(A)** Surface area of the SARS-CoV-2 stem peptide is shown. Solvent exposed and buried  
1118 areas were calculated with Proteins, Interfaces, Structures and Assemblies (PISA) (91).  
1119 **(B)** The SARS-CoV-2 stem peptide inserts into a hydrophobic groove formed by the  
1120 heavy and light chains of CC40.8. Surfaces of CC40.8 are color-coded by hydrophobicity  
1121 [calculated by Color h ([https://pymolwiki.org/index.php/Color\\_h](https://pymolwiki.org/index.php/Color_h))].  
1122 **(C)** Electrostatic surface potential of the CC40.8 paratope is shown. Electrostatic potential  
1123 was calculated by APBS and PDB2PQR (93, 94).  
1124  
1125



**B** \*Residues conserved in SARS-CoV-2, SARS-CoV, HKU1, and OC43; Green: peptide; Orange: HC; Yellow: LC



1126  
1127 **Fig. S6. Contribution of CC40.8 bnAb heavy and light chain germline and somatic**  
1128 **mutated V-gene residues in S2 stem epitope recognition.**

1129 **(A)** Alignment of CC40.8 with germline VH3-23 and VL3-10 sequences is shown.  
1130 Paratope residues [defined as buried surface area (BSA) > 0 Å<sup>2</sup> as calculated by PISA  
1131 (91)] are highlighted with yellow boxes. Somatic mutated residues as calculated by  
1132 IgBLAST (95) are highlighted in red.

1133 **B.** Detailed interactions between CC40.8 Fab and the SARS-CoV-2 stem peptide are  
1134 shown. Heavy and light chains of CC40.8 are shown in orange and yellow, while the  
1135 SARS-CoV-2 stem peptide is in pale green. Hydrogen bonds and salt bridges are  
1136 represented by black dashed lines. Somatic mutated residues are shown in red.  
1137 Conserved residues among coronaviruses are indicated by asterisks (\*).

		Alanine scanning of SARS-CoV-2 Spike													
SARS-CoV-2		WT	P1140A	L1141A	Q1142A	P1143A	E1144A	L1145A	D1146A	S1147A	F1148A	K1149A	E1150A	E1151	
Neutralization	IC50 (ug/ml, CC40.8)	11.5	1.4	0.6	3.3	238.4	14.6	N/A	84.0	20.5	>300	0.6	24.2	>300	
	n-fold	1.0	0.1	0.1	0.3	20.7	1.3	N/A	7.3	1.8	>26.11	0.0	2.1	>26.11	
BLI Binding	Response Value (CC40.8)	0.61	0.57	N/A	0.59	0.21	0.62	0.02	0.52	0.55	0.35	0.61	0.51	0.07	
	% change with WT	100%	95%	N/A	97%	35%	102%	4%	86%	90%	58%	101%	83%	12%	
	Response Value (S309)	0.43	0.43	N/A	0.41	0.45	0.42	0.40	0.43	0.45	0.44	0.42	0.48	0.47	
	% change with WT	100%	100%	N/A	94%	103%	97%	91%	100%	103%	101%	98%	110%	108%	
SARS-CoV-2		L1152A	D1153A	K1154A	Y1155A	F1156A	K1157A	N1158A	H1159A	T1160A	S1161A	P1162A	D1163A	V1164A	
Neutralization	IC50 (ug/ml, CC40.8)	143.1	71.0	4.4	>300	>300	4.7	4.5	6.7	1.9	6.4	11.6	16.0	6.6	
	n-fold	12.5	6.2	0.4	>26.11	>26.11	0.4	0.4	0.6	0.2	0.6	1.0	1.4	0.6	
BLI Binding	Response Value (CC40.8)	0.65	0.62	0.74	0.34	0.64	0.74	0.65	0.69	0.65	0.49	0.52	0.60	0.75	
	% change with WT	108%	102%	122%	55%	106%	122%	107%	114%	107%	81%	86%	99%	124%	
	Response Value (S309)	0.48	0.44	0.42	0.46	0.49	0.50	0.43	0.51	0.55	0.47	0.40	0.45	0.47	
	% change with WT	110%	101%	98%	107%	113%	114%	99%	117%	127%	108%	93%	103%	110%	

		Alanine scanning of SARS-CoV-1/2 S2 stem peptide												
SARS-CoV-1/2		WT	P1140A	L1141A	Q1142A	P1143A	E1144A	L1145A	D1146A	S1147A	F1148A	K1149A	E1150A	E1151
BLI Binding	Response Value (CC40.8)	3.8	3.5	3.8	3.8	3.7	3.5	0.9	3.3	3.3	2.3	3.7	3.5	0.6
	% change with WT	100%	92%	99%	99%	97%	92%	22%	86%	87%	61%	96%	91%	16%
SARS-CoV-1/2		L1152A	D1153A	K1154A	Y1155A	F1156A	K1157A	N1158A	H1159A	T1160A	S1161A	P1162A	D1163A	V1164A
BLI Binding	Response Value (CC40.8)	2.9	3.0	3.4	2.1	2.4	3.7	3.0	2.6	3.2	3.3	3.2	2.8	2.5
	% change with WT	76%	80%	89%	54%	62%	97%	79%	68%	84%	87%	83%	74%	66%

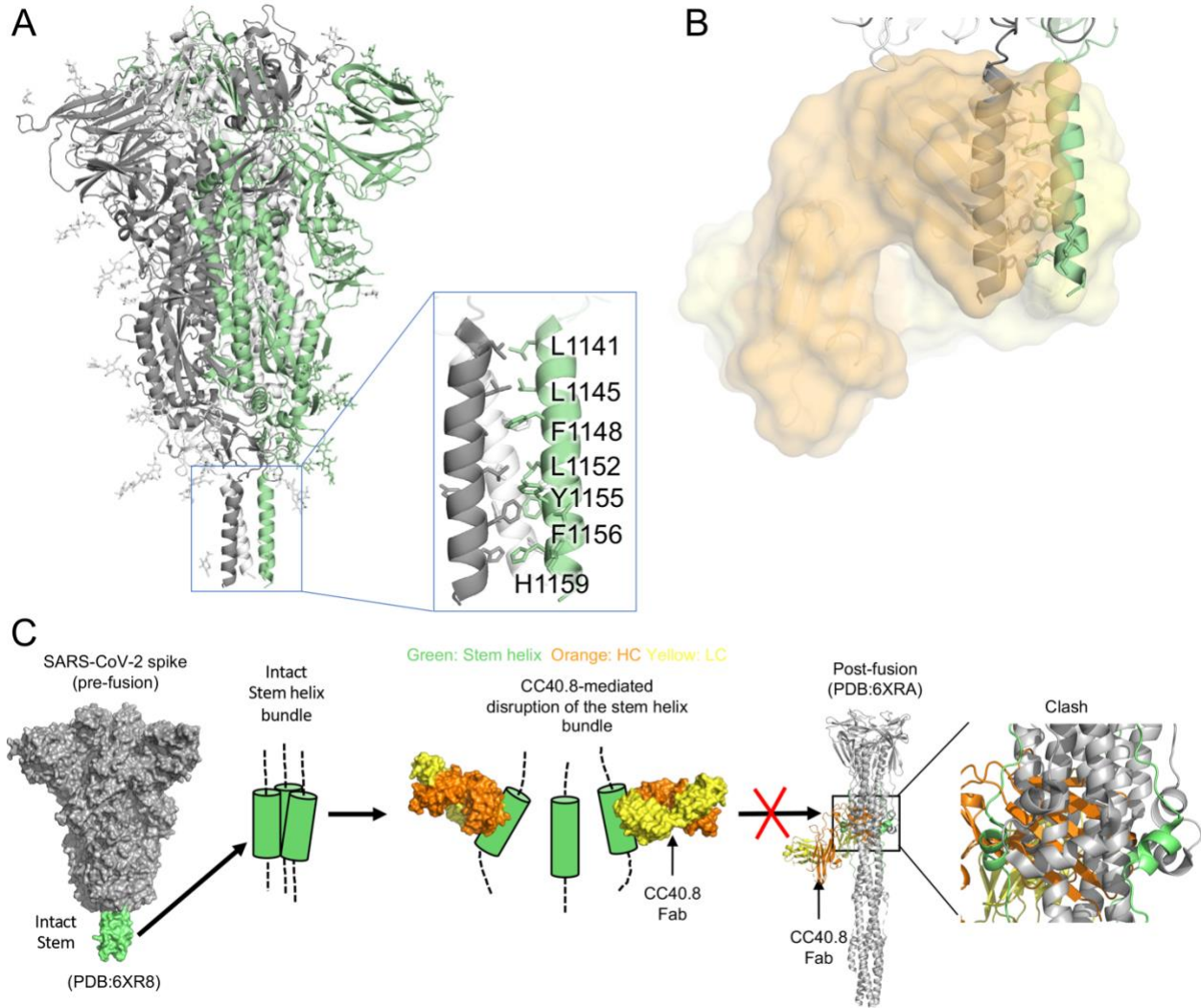
		Alanine scanning of HCoV-HKU1 S2 stem peptide												
HCoV-HKU1		WT	H1140A	S1141A	V1142A	P1143A	K1144A	L1145A	S1146A	D1147A	F1148A	E1149A	S1150A	E1151A
BLI Binding	Response Value (CC40.8)	4.2	4.6	4.3	4.4	4.4	4.4	3.3	4.4	4.0	4.0	3.6	4.0	1.7
	% change with WT	100%	110%	104%	105%	106%	105%	79%	105%	96%	96%	87%	96%	41%
HCoV-HKU1		L1152A	S1153A	H1154A	W1155A	K1156A	F1157A	N1158A	Q1159A	T1160A	S1161A	I1162A	A1163A	P1164A
BLI Binding	Response Value (CC40.8)	3.7	4.0	3.8	1.8	2.7	4.5	4.2	4.2	4.2	4.3	4.3	4.2	3.8
	% change with WT	88%	96%	91%	43%	64%	107%	101%	100%	104%	104%	104%	100%	91%

Neutralization  
n-fold <0.3  
n-fold >5

BLI Binding  
% change <80%

1138 **Fig. S7. Epitope mapping of CC40.8 bnAb by alanine scanning mutagenesis of**  
 1139 **SARS-CoV-2 spike protein and SARS-CoV-2/HCoV-HKU1 S2 stem peptides using**  
 1140 **neutralization and BLI binding assays.**  
 1141

1142 The upper panel shows the IC<sub>50</sub> neutralization of CC40.8 bnAb with wild-type (WT) SARS-  
 1143 CoV-2 and spike mutant pseudoviruses and the BLI binding responses with WT SARS-  
 1144 CoV-2 soluble spike protein and alanine mutants. SARS-CoV-2 receptor binding domain  
 1145 (RBD) antibody S309 was a control for the spike protein binding assays. The IC<sub>50</sub> fold  
 1146 change (n-fold) was calculated by dividing the mutant value by the WT value. For IC<sub>50</sub>, n-  
 1147 fold <0.3 are indicated in red, and n-fold >5 in orange. The middle and lower panels show  
 1148 BLI binding responses of CC40.8 antibody to WT and alanine mutants of the SARS-CoV-  
 1149 1/2 and HCoV-HKU1 stem-helix peptides, respectively. Binding response values where  
 1150 the % change in binding (from WT peptide) is below 80% are indicated in yellow. Antibody  
 1151 S309 that recognizes a fairly conserved epitope of the RBD of both SARS-CoV-1 and  
 1152 SARS-CoV-2 was used as control. N/A, not available.  
 1153



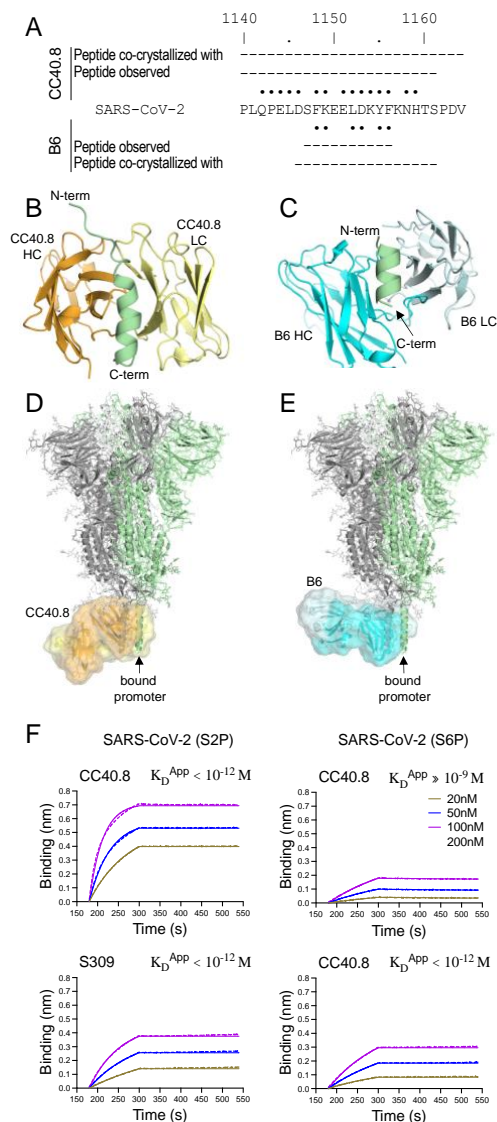
1154  
1155  
1156

**Fig. S8. CC40.8 binds to a buried interface of the 3-helix bundle: predicted mechanism of neutralization.**

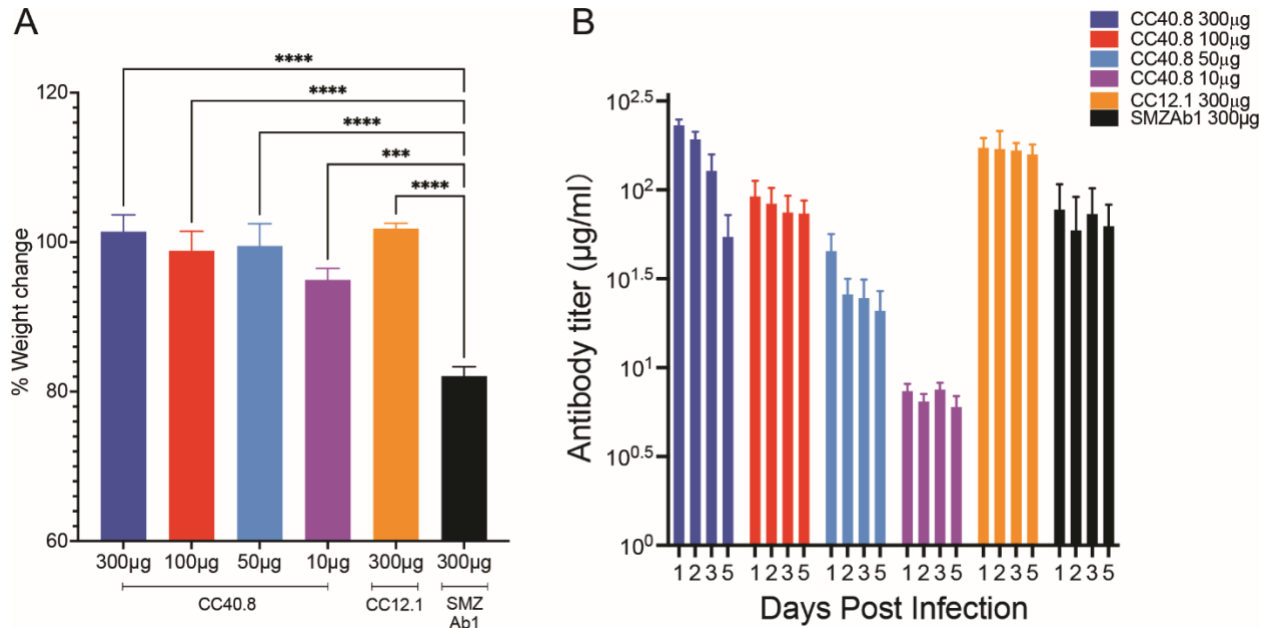
1157 **(A)** A SARS-CoV-2 spike protein structure is shown in the pre-fusion state. The three  
1158 protomers are shown in gray, pale green, and white, respectively, with N-linked glycans  
1159 represented by sticks. The 3-helix bundle stem region is highlighted in a blue-outlined  
1160 box. Representative epitope residues of CC40.8 are shown in sticks. The CC40.8 epitope  
1161 is rich in hydrophobic residues. A cryo-EM structure of SARS-CoV-2 spike protein  
1162 structure in the pre-fusion state that incorporates the coordinates of the 3-helix bundle  
1163 stem region (PDB: 6XR8, (96)) is shown here.

1164 **(B)** The SARS-CoV-2 spike protein pre-fusion structure was superimposed on the  
1165 structure of CC40.8 (orange/yellow) in complex with a SARS-CoV-2 S2 peptide. CC40.8  
1166 would clash with the other protomers of the spike protein in the pre-fusion state.

1167 **(C)** A putative neutralization mechanism of CC40.8 is presented. The S2 3-helix bundle  
1168 region is shown in green, and heavy and light chains of CC40.8 are shown in orange and  
1169 yellow, respectively. A model for the mechanism of neutralization is shown and inspired  
1170 by the interaction of a mouse S2 stem antibody, B6, isolated from a spike protein  
1171 vaccinated animal that targets a similar stem epitope (52) .  
1172



1173  
 1174 **Fig. S9. Comparison of bnAbs CC40.8 and B6 that target the S2 stem helix.**  
 1175 **(A)** A comparison between S2 stem-helix peptides targeted by CC40.8 and B6 is shown.  
 1176 Peptides used for co-crystallization with CC40.8 or B6 are indicated by dashes, with the  
 1177 regions observed in the crystal structures of each study indicated. Residues involved in  
 1178 interactions with CC40.8 and B6 are indicated by black dots (cutoff distance = 4 Å).  
 1179 **(B to E)** Structures of CC40.8 and B6 were compared. The heavy and light chains of  
 1180 CC40.8 are colored in orange and yellow, respectively, and those for B6 are in cyan and  
 1181 light cyan. The S2 stem-helix peptides are shown in green. In panels (D) and (E), a SARS-  
 1182 CoV-2 spike protein pre-fusion structure (PDB 6XR8) is superimposed on structures of  
 1183 CC40.8 and B6 in complex with a SARS-CoV-2 S2 peptide in the green protomer  
 1184 (indicated by arrows). Both CC40.8 and B6 would clash with the other protomers of the  
 1185 spike protein in pre-fusion state.  
 1186 **(F)** BLI binding kinetics of CC40.8 to S2- and S6- stabilized SARS-CoV-2 spike trimers  
 1187 are shown. An RBD-targeting neutralizing Ab S309 (97) was used as a control. Apparent  
 1188 binding constants ( $K_D^{App}$ ) of antibodies with spike proteins are shown. The raw  
 1189 experimental curves are shown as dash lines, while the solid lines are the fits.

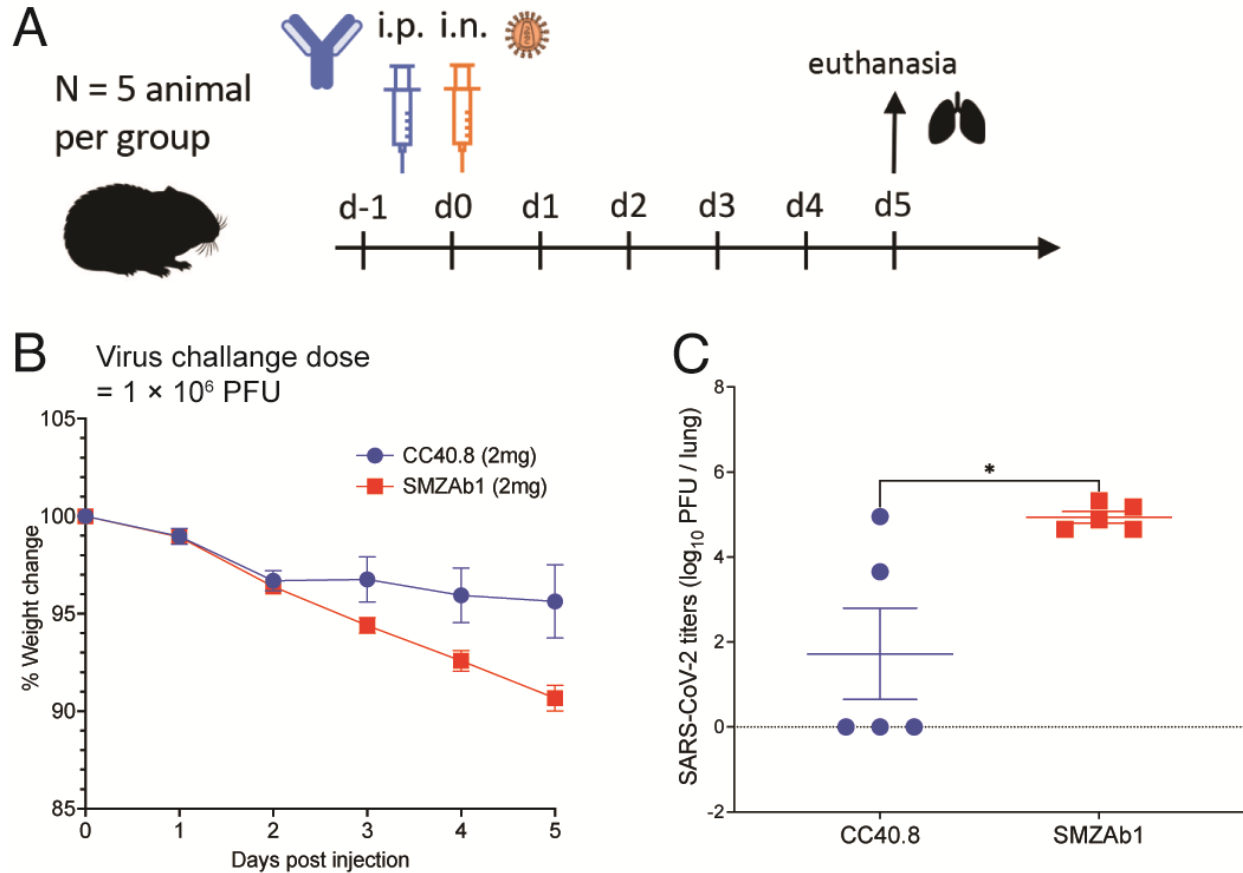


1190  
1191  
1192  
1193  
1194  
1195  
1196  
1197  
1198

**Figure S10. Weight loss, viral titers, and serum antibody titers were measured in hACE2 mice passively administered CC40.8.**

**(A)** Percent day 5 weight change was calculated from day 0 for all animals. Data are presented as mean  $\pm$  SEM. Significance was calculated with Dunnett's multiple comparisons test between each experimental group and the ZIKV Ab (SMZAb1) control group (\*\* $P < 0.001$ , \*\*\*\* $P < 0.0001$ ).

**(B)** Serum human IgG concentrations of CC40.8, CC12.1 and SMZAb1 were assessed by ELISA at day 1, 2, 3, and 5 post infection. Data are presented as mean  $\pm$  SEM.



1199  
1200  
1201  
1202  
1203  
1204  
1205  
1206  
1207  
1208  
1209  
1210  
1211  
1212  
1213  
1214

**Fig. S11. CC40.8 reduces weight loss and lung viral load and viral replication following SARS-CoV-2 challenge in Syrian hamsters.**

(A) CC40.8 was administered intraperitoneally (i.p.) at a 2 mg per animal dose into Syrian hamsters (average: 16.5 mg/kg). Control animals received 2 mg of control SMZAb1. Each group of five animals was challenged intranasally (i.n.) 12 hours after antibody infusion with  $1 \times 10^6$  PFU of SARS-CoV-2. Animal weight was monitored daily as an indicator of disease progression and lung tissue was collected on day 5 for viral burden assessment.

(B) Percent weight change is shown for CC40.8 or control antibody-treated animals after SARS-CoV-2 challenge. Percent weight change was calculated from day 0 for all animals. Data are presented as mean  $\pm$  SEM.

(C) SARS-CoV-2 titers (PFU) were determined by plaque assay from lung tissue at day 5 after infection. Three out of 5 CC40.8-treated animals had substantially reduced viral titers compared to the SMZAb1 control antibody-treated animals. Data are presented as mean  $\pm$  SEM.

1215 **Table S1. X-ray data collection and refinement statistics.**

<b>Data collection</b>	CC40.8 Fab + SARS-CoV-2 S2 peptide
Beamline	SSRL12-1
Wavelength (Å)	0.97946 Å
Space group	P 2 <sub>1</sub> 2 <sub>1</sub>
Unit cell parameters	
a, b, c (Å)	54.9, 63.7, 122.0
α, β, γ (°)	90, 90, 90
Resolution (Å) <sup>a</sup>	50.0-1.62 (1.65-1.62)
Unique reflections <sup>a</sup>	54,176 (4,897)
Redundancy <sup>a</sup>	4.3 (3.0)
Completeness (%) <sup>a</sup>	97.0 (89.6)
<I/σI> <sup>a</sup>	29.9 (1.0)
R <sub>sym</sub> <sup>b</sup> (%) <sup>a</sup>	7.9 (>100)
R <sub>pim</sub> <sup>b</sup> (%) <sup>a</sup>	2.8 (47.7)
CC <sub>1/2</sub> <sup>c</sup> (%) <sup>a</sup>	99.4 (56.3)
<b>Refinement statistics</b>	
Resolution (Å)	29.1-1.62
Reflections (work)	54,129
Reflections (test)	1,997
R <sub>cryst</sub> <sup>d</sup> / R <sub>free</sub> <sup>e</sup> (%)	17.4/20.6
No. of atoms	3,836
Fab	3,159
Peptide	193
Ligands	35
Solvent	459
Average B-values (Å <sup>2</sup> )	28
Fab	26
Peptide	34
Ligands	56
Solvent	39
Wilson B-value (Å <sup>2</sup> )	23
<b>RMSD from ideal geometry</b>	
Bond length (Å)	0.006
Bond angle (°)	1.22
<b>Ramachandran statistics (%)<sup>g</sup></b>	
Favored	98.2
Outliers	0.0
<b>PDB code</b>	7SJS

<sup>a</sup> Numbers in parentheses refer to the highest resolution shell.

<sup>b</sup>  $R_{sym} = \sum_{hkl} \sum_i |I_{hkl,i} - \langle I_{hkl} \rangle| / \sum_{hkl} \sum_i I_{hkl,i}$  and  $R_{pim} = \sum_{hkl} (1/(n-1))^{1/2} \sum_i |I_{hkl,i} - \langle I_{hkl} \rangle| / \sum_{hkl} \sum_i I_{hkl,i}$ , where  $I_{hkl,i}$  is the scaled intensity of the  $i^{\text{th}}$  measurement of reflection h, k, l,  $\langle I_{hkl} \rangle$  is the average intensity for that reflection, and  $n$  is the redundancy.

<sup>c</sup> CC<sub>1/2</sub> = Pearson correlation coefficient between two random half datasets.

<sup>d</sup>  $R_{cryst} = \sum_{hkl} |F_o - F_c| / \sum_{hkl} |F_o| \times 100$ , where  $F_o$  and  $F_c$  are the observed and calculated structure factors, respectively.

<sup>e</sup>  $R_{free}$  was calculated as for  $R_{cryst}$ , but on a test set comprising 5% of the data excluded from refinement.

<sup>g</sup> From MolProbity (98).

1216  
1217  
1218  
1219  
1220  
1221  
1222  
1223

1224 **Table S2. Demographic information of COVID-19 convalescent donors.**

	<b>COVID donor (n = 60)</b>
<b>Age (years)</b>	20 to 72 (median = 46)
<b>Gender</b>	
Male	47% (28/60)
Female	53% (32/60)
<b>Race/Ethnicity</b>	
White, non-Hispanic	80% (48/60)
Hispanic	8.3% (5/60)
Black, non-Hispanic	1.7% (1/60)
Asian, non-Hispanic	3.3% (2/60)
Unknown	6.7% (4/60)
SARS-CoV-2 PCR Positivity	75% (45/60)
Lateral Flow Positivity	60% (36/60)
<b>Disease Severity</b>	
Mild	56.7% (34/60)
Mild to Moderate	6.7% (4/60)
Moderate	25% (15/60)
Moderate to Severe	5% (3/60)
Severe	5% (3/60)
Critical	1.7% (1/60)
<b>Symptoms</b>	
Cough	60% (36/60)
Fever	55% (33/60)
Fatigue	38.3% (23/60)
Anosmia	31.7% (19/60)
Dyspnea	26.7% (16/60)
Diarrhea	16.7% (10/60)
Days Post Symptom Onset at Collection	6 to 90 (median = 35.5)

1225

1226

1227

1228

1229